Plant Physiology Preview. Published on November 18, 2013, as DOI:10.1104/pp.113.228874

Running Head: **GCR1 predicted to have a GPCR fold**

Prof Christopher A Reynolds

School of Biological Sciences

Wivenhoe Park

Colchester

CO7 9SJ

United Kingdom

Research Area:

Membranes, Transport and Biogenetics

or

Signaling and Response

Structure and functional motifs of GCR1, the only plant protein with a GPCR fold?

Bruck Taddese[1], Graham J.G. Upton[2], Gregory R Bailey[1], Siân R.D. Jordan[1], Nuradin Y. Abdalla[1], Philip J Reeves[1] and Christopher A Reynolds[1]*

[1]School of Biological Sciences, University of Essex, Wivenhoe Park, Colchester, CO4 3SQ, United Kingdom. and [2]Department of Mathematical Sciences, University of Essex, Wivenhoe Park, Colchester, CO4 3SQ, United Kingdom. Email:reync@essex.ac.uk

One sentence summary

GCR1 shares the fold and key functional motifs of class A, class B and class E GPCRs

Present address: Bruck Taddese, CNRS, UMR 6214, INSERM 1083, Fac. Med., Angers, France

Abstract

Whether GPCRs exist in plants is a fundamental biological question. Interest in deorphanizing new G protein coupled receptors (GPCRs), arises because of their importance in signaling. Within plants, this is controversial as genome analysis has identified 56 putative GPCRs, including GCR1 which is reportedly a remote homologue to class A, B and E GPCRs. Of these, GCR2, is not a GPCR; more recently it has been proposed that none are, not even GCR1. We have addressed this disparity between genome analysis and biological evidence through a structural bioinformatics study, involving fold recognition methods, from which only GCR1 emerges as a strong candidate. To further probe GCR1, we have developed a novel helix alignment method, which has been benchmarked against the the class A – class B - class F GPCR alignments. In addition, we have presented a mutually consistent set of alignments of GCR1 homologues to class A, class B and class F GPCRs, and shown that GCR1 is closer to class A and /or class B GPCRs than class A, class B or class F GPCRs are to each other. To further probe GCR1, we have aligned transmembrane helix 3 of GCR1 to each of the 6 GPCR classes. Variability comparisons provide additional evidence that GCR1 homologues have the GPCR fold. From the alignments and a GCR1 comparative model we have identified motifs that are common to GCR1, class A, B and E GPCRs. We discuss the possibilities that emerge from this controversial evidence that GCR1 has a GPCR fold.

Introduction

There has been much interest in the identification of novel GPCRs from genome analysis, initially from the human genome because GPCRs are highly druggable therapeutic targets, and more recently from other genome studies because GPCRs are vital signaling molecules in diverse organisms. Whether GPCRs exist in plants is therefore a fundamental biological question.

Here our focus on putative plant GPCRs was initiated with the characterization of GCR1 as an orphan GPCR that binds to the plant G-protein GPA1 and which is involved in the drought response (Hooley 1999;Pandey and Assmann 2004). This observation was followed by intense efforts to identify other plant GPCRs (Moriyama et al. 2006;Liu et al. 2007;Gookin et al. 2008;Pandey et al. 2009). For well-established GPCRs, there are two main classification systems. The GRAFS system (Fredriksson et al. 2003) described five classes of human GPCRs which include Glutamate, Rhodopsin, Adhesion, Frizzled/Taste2, and Secretin. Kolakowski, Attwood and Findlay (Kolakowski, Jr. 1994;Attwood and Findlay 1994) described 6 classes, namely A – E and the Frizzled GPCRs (Class F) that additionally include class D (Eilers et al. 2005) found in fungi and Class E cAMP receptors associated with *Dictyostelium* (Williams et al. 2005); the Adhesion and Secretin receptors, which differ primarily in their N termini (Lagerstrom and Schioth 2008), together form class B. GCR1 is particularly interesting from a bioinformatics perspective as it has identifiable but distant homology to class E, class B and class A GPCRs (Pandey and Assmann 2004) and so has been used to inform the medically important class A – class B GPCR alignment (Vohra et al. 2007;Vohra et al. 2013). GCR1 and the other putative plant GPCRs do not naturally fall into the well-characterized GPCR classes, as presented at the GPCRDB (Horn et al. 2003;Vroling et al. 2011) or elsewhere and so confirmation that GCR1 is a GPCR is difficult. Indeed, the pitfalls of GPCR identification are illustrated by the high profile (Liu et al. 2007) but erroneous identification of GCR2 as a plant GPCR. It has now been confirmed through crystallization that GCR2 is a lantibiotic cyclase-like protein (Chen et al. 2013), as predicted by our fold recognition studies (Illingworth et al. 2008). We are particularly interested in these putative GPCRs to assess whether as remote homologues they may similarly be used to address the difficult issue of alignment between GPCR families. In this respect only GCR1 is useful, as the fold recognition studies indicate GCR1 is the most likely candidate to have a GPCR fold while the evidence for other plant GPCRs is at best minimal. While many methods have been used to align GPCRs from different classes (Frimurer and Bywater 1999;Sheikh et al. 1999;Bissantz et al. 2004;Miedlich et al. 2004;Eilers et al. 2005;Kratochwil et al. 2005;Dong et al. 2007;Coopman et al. 2011;Gregory et al. 2013), it has not been possible to validate these methods on GPCRs until recently. However, with the recent publication of the structure of the class B glucagon receptor (Siu et al. 2013), the class B corticotropin

releasing factor 1 receptor (Hollenstein et al. 2013), and the class F human smoothened receptor (Wang et al. 2013) and the associated structural alignments between class A, and these remote homologues, we have been able for the first time to successfully test our new method. This method is a variation on that used to produce a well-validated class A – class B alignment (Vohra et al. 2013) in which GCR1 was used a bridge; in a follow-on article, the alignment formed the basis of a class B calcitonin receptor-like receptor (CLR) active model (Woolley et al. 2013) that was later shown to be in good agreement with the class B glucagon receptor X-ray crystal structure. Consequently, we have aligned the GCR1 homologues to class A, class B and class F and have generated comparative models of active and inactive GCR1. From the alignment, with the assistance of the models, we have identified a number of motifs that are common to GCR1, class A, class B and class E GPCRs, thus greatly increasing the evidence that GCR1 has a GPCR fold. In addition, we have provided further evidence that GCR1 homologues have the same fold as class A and class B GPCRs from variability analysis. Here we imply that the difference between a GPCR and a protein with a GPCR fold is the lack of definitive experimental evidence of conventional signaling partners.

Some bioinformatics studies have suggested that there might be about 50 plant GPCRs, but now it has been questioned as to whether there are any plant GPCRs (Urano et al. 2012;Urano and Jones 2013;Urano et al. 2013;Bradford et al. 2013), primarily because the plant G protein is self activating and does not *need* a guanine nucleotide exchange factors (GEF). One of the presentations of putative plant GPCRs is based on a hidden Markov model, trained on several hundred seven transmembrane helical (7TM) proteins taken from the GPCRDB (both well-characterized GPCRs and other 7TM proteins such as the MLO proteins); the genes were tentatively assigned as GPCRs on the basis of 7 predicted transmembrane helices (Moriyama et al. 2006). This assignment has been made against the background of the well documented and now closed debate as to whether the 7TM protein bacteriorhodopsin was a suitable template for modeling GPCRs (Hibert et al. 1993;Hoflack et al. 1994), most typified by the article of Hibert et al., entitled 'This is not a G-protein coupled receptor'. Given that a number of distinct GPCR X-ray crystal structures have become available (Congreve et al. 2011;Katritch et al. 2013;Venkatakrishnan et al. 2013), it is now possible to analyze these putative plant GPCR sequences to assess whether, in the light of new structural information, they are more or less likely to be GPCRs, and thus to move beyond the assumption implicit in Moriyama et al. (2006) that a receptor with 7 transmembrane helices is a GPCR (e.g. bacteriorhodopsin has 7 transmembrane helices but is not a GPCR) (Hibert et al. 1993).

Here our approach to analysis of the 56 putative plant GPCRs is to combine transmembrane structure prediction and sequence analysis with fold recognition methods. There are essentially two approaches to fold recognition, namely sequence-based methods, such as genTHREADER (Jones 1999b), and empirical potential-based methods, such as Threader (Jones et al. 1992;Jones 1998). The sequence-based methods have the advantage of speed and may be suitable for whole genome analysis but may not readily identify remote homologues when the sequence identity is low. The empirical

potential-based methods may be more efficient at identifying remote homologues but are generally not parameterized for membrane proteins. For this reason, we have taken a heuristic approach and have tested a variety of fold recognition methods to see if they correctly identify characteristic GPCR sequences from classes A – F, while at the same time not incorrectly assigning bacteriorhodopsin and GCR2 as GPCRs. In particular, our focus is on fold recognition methods such as I-TASSER (Zhang 2008;Roy et al. 2010) that have performed well in CASP fold recognition competitions (Moult et al. 2009). For proteins where the evidence that they are GPCRs was not convincing, the fold recognition (threading) results were used to give a preliminary indication as to which other types of membrane proteins they could be; the most likely alternatives were ion channels or transporters. The significance of this study is therefore four-fold. Firstly, it adds clarity to the field of plant GPCRs by indicating from a wide range of evidence that only GCR1 is strongly predicted to have a GPCR fold. Secondly, it provides evidence that some of the other candidates are more likely to be transporters. Thirdly, it indicates computational approaches that could be taken to follow up initial genome analysis studies to help avoid the confusion that has shrouded the plant GPCR field. Fourthly, the new alignment method has given promising results on well-validated alignments in or below the twilight zone (Doolittle 1986) and so could, with development, be used in other more general applications. In addition, we discuss the implications of these results that are difficult to reconcile with current knowledge of the mechanism of the *Arabidopsis* G protein, GPA1.

Methods

Transmembrane helix prediction. The putative plant GPCRs were taken from (Moriyama et al. 2006) via the Kyoto Encyclopedia of Genes and Genomes (KEGG) website (Kanehisa and Goto 2000;Kanehisa et al. 2010), along with the sequences of GTG1 and GTG2 (Pandey et al. 2009), which are also putative plant GPCRs. Transmembrane helix prediction was carried out using TMHMM 2.0 (Moller et al. 2001;Krogh et al. 2001), since we have found this to be reliable for GPCRs in general and for our controls in particular (see below). This was carried out for two purposes. Firstly, to confirm that the sequences were indeed predicted to be 7TM proteins and secondly to identify large extracellular or cytosolic domains that could be separated to increase the efficiency of subsequent fold recognition steps carried out on the individual domains (See Table S1). Since TMHMM is not 100% reliable (Melen et al. 2003;Inoue et al. 2005;Kahsay et al. 2005), we have used other well-regarded methods such as HMMTOP (Tusnady and Simon 1998;Tusnady and Simon 2001), MEMSAT3 (Jones et al. 1994;Jones 2007) and TOPpred2 (Claros and Von 1994) on proteins predicted to have other than 7TM helices. The TMLOOP (Viklund et al. 2006), OCTOPUS and SPOCTOPUS (Viklund and Elofsson 2008;Viklund et al. 2008) severs were used to predict re-entrant loops and signal peptides since re-entrant loops are not a common feature of GPCRs, except perhaps for extracellular loop 2

(ECL2) in rhodopsin which is weakly re-entrant (Palczewski et al. 2000), and signal peptides can present as transmembrane helices. However, it should be noted that re-entrant loop prediction is currently not very reliable.

Sequence similarities. Because some of the proteins, e.g. MtN3, form distinct homologous groups (Table S2), the results were analyzed in the light of the results for other members of the same family as they are either all GPCRs or all not GPCRs. Moreover, if they are not GPCRs then they should all belong to the same alternative family.

Fold recognition. The well-characterized GPCRs and related sequences used as positive controls were A4D2G4_HUMAN (olfactory 2, class A), Q8IV17_HUMAN (Secretin receptor, class B), B0UXY7_HUMAN ($GABA_B$ subtype1, class C), Q6TMC6_COPCI (pheromone receptor, class D), CAR3_DICDI (cyclic AMP receptor 3, class E) and FRIZ2_DROME (frizzled 2, class F). The negative controls were AAU04564.1 Halobiforma lacisalsi (bacteriorhodopsin) and AT2G20770 (*Arabidopsis* GCL2 GCR2). Bacteriorhodopsin is a 7TM protein but not a GPCR while GCR2 has 7 hydrophobic helical motifs that are almost long enough to span the membrane so that its homologues were initially erroneously identified as GPCRs (Illingworth et al. 2008). These sequences were submitted to the following fold recognition servers: I-TASSER (Roy et al. 2010), FUGUE (Shi et al. 2001), Phyre (nett-Lovsey et al. 2008), genTHREADER (Jones 1999a), mgenTHREADER (McGuffin and Jones 2003), HHpred (Soding et al. 2005), LOMETS (Wu and Zhang 2007) and MUSTER (Wu and Zhang 2008). Generally, each server gives a key metric, such as a Z-score, and an associated interpretation such as 'high', 'medium' or 'low', that indicates the expected reliability of the result. It is understood that fold recognition methods do not necessarily give the correct fold as the highest ranked hit and so we have looked for the correct fold from the controls to be given in the top 10 hits.

Transmembrane Helix alignment. The alignment between GCR1/class E and class A and class B GPCRs was previously determined on a helix by helix basis by combining (via a product of scaled scores) the results of a profile alignment with maximum lagged correlation. The alignment was evaluated over a well-defined transmembrane region in which the internal/external character of the residues was invariant over a number of class A GPCR structures; the profile contained a flank of 8 residues either side of this region (Taddese et al. 2012) but flanks of 15 residues were investigated to ensure that 8 was sufficient; the averaging and scaling of the individual alignment scores or correlation coefficients between 0 and 1 ensured that the noise was minimized and allowed the correct alignment to appear above the noise (Vohra et al. 2013). Here we have replaced the profile alignment with an ungapped pairwise alignment of all possible pairs of sequences of each class; the best alignment for a given helix being taken as the most common alignment (Fig. 1). Here the alignments

were scored using the PHAT substitution matrix (Ng et al. 2000) that was specifically derived for transmembrane helices; they were also scored using the widely used Blosum62 substitution matrix (Henikoff and Henikoff 1993) to check that the results are not unduly sensitive to the choice of matrix; Blosum62 was used in the previous study. (There are problems with the derivation of the Blosum62 matrix, but these actually serve to enhance its performance in searches (Styczynski et al. 2008)). For the hydrophobicity, we have carried out maximum lagged correlation, not of the average hydrophobicity as previously, but for every pair of sequences (one from each class), with the best alignment for each pair of sequences given by the highest correlation coefficient. The best alignment was again being taken as the most common alignment, i.e. the one that received the most 'votes' (Fig. 1). In addition, we have included amino acid volume (Sandberg et al. 1998) as an additional property that was treated in the same way as the hydrophobicity. Thus for the substitution matrix, for hydrophobicity and for volume, each ungapped alignment (-1, 0, +1 etc) received a number of votes according to the number of times that it received the highest score. However, in the subsequent step, it was the number of votes that were scaled between 0 and 1 rather than the scores. Entropy is a property of every sequence in the alignment, so we have retained the maximum lagged correlation of the entropy. As before, the scores were averaged over the forward and backward alignments, scaled between 0 and 1 and the 4 scores were multiplied together to give an overall score that gives an indication of the preferred alignment. Each of the 4 methods may indicate a different alignment, but the benefit of scaling the measures between 0 and 1 and multiplying them together is that alignments receiving little support are suppressed while alignments receiving multiple support are enhanced. For remote homologues, some measures may occasionally receive a score near 0 and to check for this the product was also generated 3 more times, with either hydrophobicity, volume or entropy omitted.

For comparative purposes, we have also generated the alignments using AlignMe in default mode via the web (Stamm et al. 2013). For these alignments to be a fair comparison the first profile (e.g. class A) included the 16 flanking residues while the second profile (e.g. class B) omitted these; the reverse alignment (i.e. omitting the flanking residues for class A) was also performed; standard prolife alignments were also performed.

We have also used the new method to assess the transmembrane helix 3 (TM3) alignment between GCR1/class E and all other GPCR classes, as defined at the GPCRDB (www.gpcr.org/7TM_old/); we focused on TM3 since its alignment is more straightforward than that of other helices for class A – class B – GCR1/class E and so it seemed reasonable to expect this to carry over to other GPCR classes (Vohra et al. 2013). The class C, class D and class F multiple sequence alignments for TM3 included 464, 39 and 107 sequences and were prepared as described previously (Vohra et al. 2013); class F GPCRs, like class A and class B are believed to have evolved from class E GPCRs (Krishnan et al. 2012;Chabbert et al. 2012) and have some homology to GCR1 (Pandey and Assmann 2004). In addition to the combined alignment for GCR1/class E, we also repeated the work using sequences in the GCR1 plant group (PR02000), as defined by the PRINTS

database (Attwood et al. 2012); despite the small number of unique sequences (9), this gave essentially the same results, except for class C. For convenience, the PRINTS class A (PR00327) and class B (PR00249) alignments were also analyzed.

Our use of the Ballesteros and Weinstein numbering system (Ballesteros and Weinstein 1995) is defined in (Vohra et al. 2013).

Variability

Baldwin's alpha carbon template (Baldwin et al. 1997) derived primarily from the rhodopsin electron cryomicroscopy map was widely used until the first GPCR X-ray crystal structure was published (Palczewski et al. 2000); its reliability was in part due to the incorporation of variability. Variability is very sensitive to the micro-environment of a residue within the helical bundle and hence it is able to report on the fold: families with a similar fold should have similar patterns in variability. Most notably, external residues should have high variability while internal residues should have low variability. Our method for determining variability is given in the supporting information of (Vohra et al. 2013). For the GCR1 homologues, analysis of 191 sequences on a helix by helix basis resulted in 42, 47, 19, 40, 49, 30 and 34 subsets for TM1 – TM7 respectively. We have compared the variability to that of class A and class B GPCRs, which was reported previously (Vohra et al. 2013). In addition, variability was used as an alternative to entropy in the transmembrane helix alignments.

Alignment quality

For the alignment of remote GPCR homologues, it has been proposed that while equivalent residues may differ in identity and properties, the position of functionally important residues is likely to be conserved (Frimurer and Bywater 1999); this 'cold spot' method has formed the basis of many class B and class C GPCR models. Here, an indication that a given helix alignment could have arisen by chance was assessed by equation (1)

$$Q = \sum_{i=1}^{N} (S_G(i) - S_X(i))^2 \qquad (1)$$

where $S_G(i)$ is the entropy of position i in a given GCR1/class E helix and $S_X(i)$ is the entropy of the corresponding class A or class B residues; the sum is evaluated over the N helical residues of the alignment window. This was compared to the distribution of values generated when the target sequences were compared with other potentially relevant sequences. These latter were observed sequences taken from other helices and from other classes (i.e. for TM1 of GCR1 homologues, the 'random' or rather comparator sequences were taken from TM2 – TM7 of classes A, B and F). This choice ensured that the comparison was with sequences possessing relevant properties such as hydrophobicity, secondary structure, periodicity and conservation. For this purpose, the mid points of

the comparator helices were aligned to the mid points of the reference helix and a total of 11 sequences generated by shifting the comparator helix by ≤±5 residues (to give a reasonable number of residues with an even radial distribution). There are caveats in this approach. Firstly, we have assumed that the functional residues can be equated with low entropy (though the mathematic approach uses all entropy values). Secondly, the validity of the 'cold spot' method has not been fully validated. Thirdly, the comparator helices may be distantly related by evolution. (An alternative approach to this problem involving group conserved residues (Eilers et al. 2005) is described in Table S13 but the entropy-based approach is superior because it uses the full range of conservation data for all residues in the helix.)

GCR1 Comparative model. The *Arabidopsis* GCR1 (TAIR locus ID At1g48270, 288 amino acids) sequence was obtained from the Kyoto Encyclopaedia of Genes and Genomes (KEGG) website (Kanehisa and Goto 2000;Kanehisa et al. 2006;Kanehisa et al. 2010). Nine Class A X-ray crystal structures of the β_1-AR (PDB code: 2VT4)(Warne et al. 2008), rhodopsin (1U19)(Palczewski et al. 2000), the adenosineA_{2A}R (3EML)(Jaakola et al. 2008), dopamine D_3R (3PBL)(Chien et al. 2010), muscarinic M_2R (3OUN)(Haga et al. 2012), histamine H_1R (3RZE)(Shimamura et al. 2011), sphingosine $S1P_1$R (3V2W)(Hanson et al. 2012), the chemokine CXCR4 (30DU)(Wu et al. 2010), protease activated receptor 1 (3VW7)(Zhang et al. 2012), two class B crystal structures of the corticotropin releasing factor 1 receptor (4K5Y)(Hollenstein et al. 2013) and the glucagon receptors (4L6R)(Siu et al. 2013) and the class F structure of the smoothened receptor (4JKV)(Wang et al. 2013) were used as templates (see Fig. 2 for the alignment, which was originally derived from a structural superposition of the structures using Modeller and which is consistent with the transmembrane helix alignment, see below). Here we used multiple templates to generate a single inactive GCR1 model because it is generally appreciated that the use of multiple templates results in better comparative models (Taddese et al. 2013). For class F, alternative TM6 and TM7 alignments can be derived depending on how the structural alignment is performed, but these alternatives did not affect the Modeller results (results not shown), presumably because of the low percentage identity to class F GPCRs in TM6 and TM7.

The models were ranked according to their DOPE (Discrete Optimised Protein Energy) assessment score (Eswar et al. 2006). From these highest scoring models, the one with the least amount of helical distortion in the transmembrane region was selected using the secondary structural assessment as implemented in VMD (Humphrey et al. 1996). This essentially amounted to ensuring that the distortion due to the class A TM2 proline was not transmitted to the GCR1 models. The inactive models were also selected on the basis of an ECL2 conformation that was similar to that in one of the class B GPCR structures, since GCR1 homologues share the ECL2 CW motif with class B GPCRs. The intracellular and extracellular loops were refined in Modeller using the Modeller loopmodel function, and the structure with the lowest DOPE score was selected. A similar loop-

refinement strategy, combined with experimental mutagenesis, gave rise to the prediction of a CLR ECL2 conformation that was later shown to be similar to that in the glucagon receptor (Woolley et al. 2013). However, it must be stressed that loop modeling is difficult and that major indeterminations will reside in the loop regions. The models were used in conjunction with the alignments and class A and class B structures to identify common motifs.

Results and Discussion

Control sequences

The fold recognition results for the 6 control sequences are given in Table S3. For each server, the negative controls bacteriorhodopsin and GCR2 were correctly identified as bacteriorhodopsin and a protein of the LanC synthase family respectively. The class A sequences were readily identified because the templates in the database were also from class A. Classes B and E were also generally identified strongly whereas classes C and F appear to be the most difficult to identify. Nevertheless, the I-TASSER, mgenTHREADER, LOMETS, HHpred and Phyre methods all identified class C and F GPCRs with reasonable confidence, albeit in the top 4 hits rather than in the top ranked hit for a few cases. The general ranking of these methods for this problem appears to be I-TASSER > LOMETS > HHpred > FUGUE > Phyre > mgenTHREADER > MUSTER > genTHREADER. The score at which the first incorrect result occurs is an important marker. Some methods do not report an incorrect result (e.g. Bacteriorhodopsin submitted to Phyre or GCR2 submitted to HHpred) and for these methods the lowest score for a correct result also provides a useful guide; these scores are given in Table S4. Thus, the Phyre results are deceptively good as all sequences were identified at rank 1 with 100% certainty. However, Phyre also identified ion channels and transporters as lower-ranked hits with 95% certainty for class A GPCRs – for this reason only Phyre results reported with 100% certainty are included in Tables 1 and 2. LOMETS also reported two results that are below the level of certainty provided by the controls and so these are also omitted from the results given in Tables 1 and 2. The full set of Phyre results is given in Table S5. The performance of I-TASSER, LOMETS, HHpred, FUGUE and Phyre on this particular problem was superior to that of the other methods so further analysis was restricted to these.

Transmembrane helix prediction

The 16 putative GPCR sequences (Moriyama et al. 2006;Pandey et al. 2009) that were not predicted to be 7TM proteins by TMHMM are recorded in Table S6. Nine were subsequently predicted by more than two methods to be 7TM proteins; 7 were predicted not be 7TM proteins by more than four methods (underlined in Tables 1 and 2 with the probable number of TMs given in parenthesis). Proteins At5g37310 and At5g62130 have been predicted by SPOCTOPUS and MEMSAT to have an

N-terminal signal peptide instead of the first predicted TM helix. Therefore, At5g37310 is assumed to have 9TMs instead of 10TMs and At5g62130 may have 7TM instead of 8TM. The OCTOPUS server has only predicted At5g62960, a member of Expressed protein family 2 (Table 1), to have a re-entrant loop (originating from inside, between residues 248 to 255 that are predicted to lie between TM5 and TM6). Since re-entrant loops are not a common feature of GPCRs (except perhaps for ECL2 in rhodopsin or the smoothened receptor), this may implicate a different super-family such as transporters.

Fold recognition

Overall results. The fold recognition (threading) results for the putative GPCRs are given in Tables 1 and 2. Threading hits from the I-TASSER server (a reliable server according to the CASP fold recognition competition (Moult et al. 2009)) indicate that GCR1 is the only candidate that is strongly predicted to have a GPCR fold. The LOMETS server has predicted two putative plant GPCRs, GCR1 and At2g01070, with high confidence and two (At5g19870 and At5g13170) with low confidence. At2g01070 aligns with the Lung 7TM receptors (PFAM code PF06814), which have homologues in plants, invertebrates, fungi and mammals. As yet there is no evidence that these proteins are GPCRs but A2g01070 was predicted by three servers. All members of the lung 7TM family have GPCR hits including *Q22938_CAEEL* by I-TASSER, and all members were predicted to be GPCRs by HHpred, some with high confidence. The HHpred server has indicated that 7 other putative plant GPCRs sequences are likely to be GPCRs albeit with low confidence except for GCR1. FUGUE indicates that 6 of the 54 sequences are likely to be GPCRs. However, apart from GCR1, the GPCR hits were reported below the cutoff. The Phyre server gave two GPCR hits with 100% confidence: GCR1 and At2g01070, which was also weakly predicted by HH-pred (the Phyre homology search is driven by HH-pred).

As a result of this analysis, there is additional evidence that 12/56 proteins could be GPCRs since they have been identified by one or more fold recognition servers. There is also additional evidence that 44/56 proteins are less likely to be genuine GPCRs since they were not identified as having a GPCR fold by any of the fold recognition servers. In addition, since only 3 of the 7 MLO proteins are predicted (very weakly) to be GPCRs and the remaining 4 are not, it seems reasonable to assume that none of the MLO proteins are GPCRs (since a homologous family should all have the same identity). Urano and Jones dismissed the MLO proteins as GPCRs primarily because their role in conferring fungal resistance is independent of G proteins (Urano and Jones 2013). Similarly, it is most likely that none of the Nodulin MtN3 proteins are GPCRs, especially as MtN3 non-plant proteins are 3TM proteins (PFAM code PF03083) that have high similarity (~85% identity) to TM1-3 and TM5-7 of their plant relatives. Such symmetry between TM1-3 and TM5-7 would not occur in a classic GPCR and so the MtN3 putative plant GPCRs are similarly unlikely to be GPCRs. We note that symmetry does occur in transporter families. GTG1 and GTG2 and the three groups of

'Expressed protein' families (Table 1) are similarly ruled out by the homologous family argument. GTG1 and GTG2 are particularly suspected as they seem to have the wrong number of transmembrane helices to be GPCRs. Within Table 1, the only families where the fold recognition results indicate that they could be GPCRs is the TOM3 family and the lung 7TM proteins since every member of the family has been implicated and there is evidence from more than one server. For the proteins in Table 2, we note that only GCR1 is predicted to be a GPCR by more than one method. In conclusion, the most likely GPCRs, besides GCR1, are At2g01070 and the TOM3 family. However, apart from GCR1, the results are far from conclusive. Four other possible GPCR candidates are listed in Table 3, with the final list of 9 proteins reduced from 12 by homology arguments.

GCR1 fold recognition results. Despite the additional sequences in Table 3, here we present the evidence that GCR1 is the only candidate to have a GPCR fold. All five fold recognition methods matched GCR1 to the GPCR fold. Secondly, GCR1 was used as a bridge in the well-validated class A – class B GPCR alignment (Vohra et al. 2013) that has generated a CLR model (Woolley et al. 2013) in good agreement with subsequent experimental structures (Siu et al. 2013) – this approach would probably have been ineffective if GCR1 did not have a GPCR fold. In the conclusions we summarize nine additional observations (see below) consistent with the hypothesis that GCR1 has a GPCR fold.

However, the role of GCR1 as a GPCR as been questioned (Urano and Jones 2013), firstly on the basis of a lack of homology to other GPCRs, secondly because of questions regarding its class E homologues, thirdly because of doubts about the GCR1 – G protein interaction and finally because of the observation that plant G proteins do not require GPCRs to act as GEFs (Johnston et al. 2008;Urano and Jones 2013).

Relatively few commentators doubt that class E homologues signal through G proteins (Janetopoulos et al. 2001;Ray et al. 2011;Krishnan et al. 2012;Yan et al. 2012). With regards to homology between GCR1 and other GPCRs, rather than limited homology to TM3 and TM4 of class E GPCRs as previously claimed (Urano and Jones 2013), earlier reports identified similarities to class A and class B GPCRs covering a much wider range (Josefsson and Rask 1997;Plakidou-Dymock et al. 1998). We extend this work to show (below) that there is considerable homology to all eight helices of class A and class B GPCRs. While there has been difficulty in reproducing (Urano and Jones 2013) the reported GCR1 – GPA1 interaction (Pandey and Assmann 2004), we show that GCR1 possesses motifs that would facilitate this interaction. The idea that GCR1 and G proteins can act independently (Chen et al. 2004) is not necessarily relevant as this is a property of well characterized GPCRs (Bockaert and Pin 1999;Rajagopal et al. 2010b;Whalen et al. 2011;Koval and Katanaev 2011). The final point however, i.e. whether GCR1 is a GEF, is a most noteworthy point and will be discussed below. This point lies at the heart of the question as to whether plants have GPCRs and can only be finalized by experiment. However, given that the function of GCR1 is currently unknown, it is important to assess what can be learned about GCR1 from structural

bioinformatics so that these experiments can be planned more carefully based on the known interplay between structure and function.

The class A - class B - class F alignment

Illustrating the method. Selected alignment results to illustrate the method are given in Fig. 1. Fig. (1A) shows the number of votes for each of the 17 alternative TM3 Class A – class B pairwise alignments, evaluated using both the Blosum62 matrix and the PHAT matrix. Here the Blosum62 results show that alignment 0 (the alignment inferred by superposition of the X-ray structures) is the overwhelming choice as the alternatives received very few votes. Alignment 0, is also an overwhelming choice for the PHAT matrix, but the preference of the 0 alignment over the alternatives is not quite so marked. The corresponding pairwise sequence alignment-based results for TM1, shown in Fig. 1B are more representative, in that alignment 0 receives the highest number of votes, but other alignments also receive votes; for TM1, the PHAT matrix highlights the experimentally inferred alignment (0) more strongly than the Blosum62 matrix. Overall, the performance of the two matrices is very similar: PHAT gives a cleaner preference for TM1 and TM2 while Blosum62 gives a cleaner preference for TM3 and TM4; for TM5 – TM7 there is no clear pattern. Fig. 1C shows the results for class A – class B TM7 alignment; here the method does not indicate a clear alignment choice but rather a number of different alignments are indicated. This situation can arise if the two multiple sequence alignments are too distant from each other, if the alignment contains gaps or if the alignment region is too short and key motifs have been omitted as here (for Fig. 1C the alignment was terminated prior to position 7.52 because this region of TM7 is α-helical in class A and 3_{10}-helix in class F – under such circumstances other information may be required to determine the true alignment.

Fig. (1D) shows the number of votes for each of the 17 alternative TM3 Class A – class B pairwise alignments, evaluated using both hydrophobicity and volume. For each of these measures, 0 is not the preferred alignment but the 0 alignment nevertheless receives a reasonable number of votes. It is important to note that in about a third of the cases where the alignment is known, hydrophobicity and volume gave a small number of votes to the correct alignment such that the scaled score is less than 0.5. While it is clearly important that the overall hydrophobicity profiles have a reasonable match, local variations arise between remote homologues and so hydrophobicity as used here may not always be appropriate. Only in one case out of 21 did both hydrophobicity and volume give a low number of votes to the correct alignment.

The results of the maximum lagged correlation of entropy and variability are given in Fig 1E,F for two alignments. Fig. 1E shows that entropy and variability are generally not as discriminating as hydrophobicity and volume as more alignments tend to receive a high score. In Fig. 1E entropy gives a higher score for the zero alignment while in Fig. 1F scaled variability gives a higher score. Overall the performance of these two measures is similar, but variability requires a

larger number of sequences and so may be more difficult to calculate. Occasionally, maximum lagged correlation of entropy can suggest an alternative alignment if strongly conserved residues do not align (Vohra et al. 2013). Fig. 1G shows that the product scores for the class A – class B TM3 alignment all give overwhelming support to the correct (0) alignment. Fig. 1H shows that the product scores for the class A – class B TM5 alignment all give support to the correct (0) alignment, but also indicate alternative alignments. Here we note that the scaled volume score is low, hence the high product score when this is omitted.

The class A – class B - class F alignment

The publication of the X-ray crystal structure of two class B GPCRs (Hollenstein et al. 2013;Siu et al. 2013) and a class F GPCR (Wang et al. 2013) provides the first opportunity to validate methods for aligning helices of remote GPCR homologues. Ideally, the method should reproduce the class A – class B, class A – class F and class B – class F alignments (Fig. 2) for each helix in agreement with experiment. Since these alignments are difficult, particularly those involving class F, as shown by a blind-modeling competition (Abagyan 2013), a secondary criteria is that the method should generate consistent alignments, i.e. the class B – class F alignment should be consistent with the class A – class B and class A – class F alignments and that this consistency could arise through choice of an alternative alignment that receives a reasonable score. (Consistency provides a useful control in situations where the experimental alignment is not known).

The alignments for TM1 – TM7 are given in Fig S1 – S7. For all 3 TM1 alignments, alignment 0 receives a good score and excellent results are obtained if hydrophobicity is omitted from the product for class F alignments. Fig. S1G shows that variability for the class A – class F and class B – class F 0 alignments fits better than that for the -3 and -7 alignments respectively (indicated by Fig. S1D,F) as the latter have three minima outside of the shaded area, as opposed to one: the low variability should either be in internal regions or in external regions that are tightly packed against neighboring helices; the apparent violation for the class F 0 alignment at positions 1.38 and 1.43 fit into this latter category, but the other violations do not. For TM2, TM3 and TM4, excellent agreement with experiment is achieved for all three alignments.

For TM5 – TM7, the situation is a little more difficult, partly because there are gaps reported in the class A – class F alignments. However, the reported alignment places equivalent residues in very different environments (Wang et al. 2013) and alternative structural alignments place the gaps in different positions (results not shown).

For TM5 the gap in class F alignments is outside of our alignment window and so is not a problem. The correct alignment is obtained for class A – class B (the +4 alternative aligns the conserved proline residues; Fig S5G also shows that it should be given a low weighting because it gives a minimum in variability in an external position (5.59)). The correct alignment is also given for class B – class F (where the prolines align). For class AF, the +4 alternative aligns the prolines, but

this is not consistent with experiment or the class B – class F alignment; the +4 alternative alignment also gives several variability minima in external regions and more worryingly a variability maximum in internal position 5.64. Both the class A – class F 0 and -4 alignments are consistent with the alignments to class B, i.e. the following two sets of alignments are mutually consistent (but only the first is consistent with experiment): AB: 0, AF: 0, BF: 0 and AB: 0, AF: -4, BF; -4. The class F 0 and -4 alignments are also largely consistent with the variability data as the maxima and minima are generally in external and internal positions respectively. Thus, this is an example of where additional information may be required to determine the alignment: the strongest scoring -4 alignment places a class F polar lysine at position 5.65, which is normally hydrophobic and required for G protein coupling (Vohra et al. 2013). For the 0 alternative, which has a reasonable score if volume is omitted, a conserved leucine aligns with position 5.65. Given that the class A - class B alignment is difficult (Vohra et al. 2013) and that class F is even more distant, these represent good results.

For TM6, the class A – class B alignment is reproduced well, but the class A – class F and class B – class F results are clearly not in line with the structural alignment. The simplest explanation for this is that the structural alignment places a gap in the middle of TM6 for class F and that our current alignment methods cannot easily deal with this problem. More significantly, Wang et al. (2013) place this gap at position 6.47, whereas we place this at 6.41 – the lack of a clear correspondence over such a range no doubt contributes to the difficulty of the alignment. The four high scoring class B – class F alignments (Fig. S6E) and the lack of consistency between the alignments should alert the reader that there may be a problem, even in the absence of an experimental alignment.

For TM7, the class A – class B alignment is reproduced well. There is some uncertainty as to the alignment of the intracellular end of the smoothened receptor. Our structural alignment places W535 in the same position as $Y^{7.53}$ of the NPXXY motif; we therefore place a gap at position 7.52 (Wang et al. (2013) place 5 gaps). Our class A – class F structural alignment therefore reproduces the alignment better (Fig. S7G) if the right-hand window limit is reduced to position 7.51 from position 7.53 (Fig. S7D). There is no need to shorten the window for the class A – class B alignment as there is no gap, and indeed such shortening reduces the quality of the alignment (as shown in Fig. 1C) as part of the key NPXXY motif is missing. The class B – class F alignment is reproduced provided that hydrophobicity is omitted from the product (Fig. S7F). Moreover, the class F variability for the +1 alignment has three high scores / maxima at internal positions (7.39, 7.42, 7.49), as shown in Fig. S7H. The class F variability fits the topology except at position 7.53, but this is due to the change in conformation to a 3_{10}-helix. The variability for the class F -4 alignment is compatible with the topology.

Together, the results in Fig S1–S7 show that the method is capable of aligning GPCR transmembrane helices of remote homologues, especially where allowance is made for insight from structural information and where there are no gaps in the alignment window. For some helices, the

method is very clear, but in general the procedure is not a black box method as some attention may need to be given to the role of hydrophobicity and volume and to the nature of the alternative alignments, which in some cases may be eliminated using variability. As in all alignments of remote homologues, care can be given to the alignment of motifs (Lesk 2002); this has been done elsewhere for the class A – class B alignment, which has been well-tested by mutagenesis studies (Vohra et al. 2013). While there are clearly limitations to the method, it should be appreciated that these are difficult alignments and that the web version of a recent state of the art method (Stamm et al. 2013) only correctly aligned a few of these 21 transmembrane helix pairs and did not align any pairs in a mutually consistent way; the standalone version offers more control and probably does much better. We will now apply the method to GCR1 homologues, which are not as difficult as the class A – class F and class B – class F alignments as they are less firmly in the 'twilight zone' (Doolittle 1986) of ~18-25% identity.

The alignment of GCR1 homologues

For each helix where the class A – class B – class F structural alignment is well-defined, the new alignment method generates a clear alignment in the sense that the alignment is (a) unambiguous as there is a single main peak, (b) an equivalent alignment is given to class A, class B and class F and (c) there is no need to omit hydrophobicity or volume from the product as all four measures support the preferred alignment. The exception is the TM6 class F alignment, which will be discussed below. The full results for the alignment are shown in Fig. S8 – S14 and these are summarized in Fig 3. The individual alignments to the GCR1 homologues are therefore better defined than the corresponding class A – class B – class F GPCR alignments, which are known from the structural alignments. The reason for this is probably that GCR1 homologues are generally closer to class A, class B and class F GPCRs than these are to each other. Thus, Fig. 4A (and Fig. S15) shows that the alignments involving GCR1 homologues generally have higher percentage identities, higher average matrix scores and higher product scores than the alignments between the well known GPCRs (class A, class B and class F). Analysis of Fig. 4A indicates why the alignments involving TM6 of class F are difficult (Abagyan 2013): these alignments have the lowest percentage identities (e.g. 7% for the alignment to class A) resulting in some of the lowest PHAT matrix scores and the lowest product scores (Fig. S15). (Some TM3 alignments also have low PHAT matrix scores, but for TM3 these are nevertheless much higher than the next scoring alignments while for TM6 this is not the case). To some extent, the structural alignment depends on how the superposition is carried out, but for TM6, class F residues have a greater tendency to point in different directions to their counterparts, even when the Cα atoms are in close proximity. In general, TM1 – TM4 show a closer structural superposition than TM5 – TM7 and this is in line with the greater sequence similarity shown by TM1 – TM4. The alignment of GCR1 to class A, class B and class F GPCRs is shown in Fig. 2.

Alignment of GCR1 TM3 to all known GPCR classes

Fig. S10 also shows the alignment scores between class C and class D GPCRs with GCR1 homologues for TM3, which is the structural and functional hub for GPCRs (Venkatakrishnan et al. 2013) and so it is noteworthy that the new method also gives a very strong signal for these two additional classes provided that volume is excluded, as in the original method (Vohra et al. 2013) that has yielded a model of the CGRP class B GPCR in good agreement with the class B X-ray structure of the glucagon receptor (Woolley et al. 2013).

Consequently, Fig. S16 shows a TM3 alignment of GCR1 against all known GPCR classes. While this alignment shows a degree of diversity amongst the different GPCR classes, it is clear that TM3 of GCR1 also shares many similarities, particularly with class B, class E and Frizzled/smoothened, e.g. the $CY^{3.26}$ motif, the conserved $W^{3.42}$ and the conserved aromatic residues at positions 3.33 and 3.51 – see also reference (Krishnan et al. 2012). The TM3 percentage identity between class C and class D with the GCR1 homologues are 14.3% and 11.9% respectively, giving rise to mean PHAT matrix scores of -3.6 and -6.2, suggesting that GCR1 homologues lie closer to class A, class B and class F GPCRs than to class C or the class D (fungal) GPCRs.

Variability

The variability for class A, class B and GCR1 homologues is shown in Fig. 5; class F was omitted from this analysis because of the greater divergence in sequence and structure, despite the high percentage identity to some helices. For each helix, the pattern of variability for the GCR1 homologues is very similar to that for the class A and class B sequences. For each helix, there is essentially a repeating pattern, with low variability at the internal or buried positions, e.g. positions 1.46 and 1.50 on helix 1 and high variability at the external exposed positions, e.g. positions 6.41 and 6.46 in helix 6. For such exposed positions, the maximum for GCR1 homologues generally coincides with the exposed region and usually aligns with that for class A or class B or both.

The magnitude of the variability is partly a reflection of the number of subsets used, but within each helix the qualitative patterns are generally the same for all three classes and these patterns are distinct from those for other helices. There are a small number of exceptions to the general internal/external pattern, but the deviations are small, and comparable to those observed for class B and these mainly arise from low variability at external positions that are nevertheless restrained by steric interactions with neighboring helices, e.g. position 5.57. In summary, the overall picture to arise from the variability is that the GCR1 homologues share the GPCR fold since the distinct patterns result from the GPCR fold. TM6 -4 alternative alignment (which derives from the class F alignment) is clearly incompatible with the fold because of the high variability at internal position 6.48; the variability patterns for alternative +3 and +4 alignments for TM1 and TM5 respectively do not match

the class A and class B patterns as well as the 0 alignment does, but cannot be eliminated as the mismatch is not too severe.

GCR1 motifs

Analysis of the sequence alignments (Fig. 2, Fig. S16) and the GCR1 comparative models (Fig. 4B, available from ftp.essex.ac.uk/pub/oyster/GCR1_2013/GCR1_models.tar.gz) has identified a number of motifs that are common between class A, class B GPCRs and the GCR1 homologues, as shown in Table 4. The most notable motif is the disulfide bond between the top of TM3 and ECL2, which is present in almost all GPCRs, and is characteristic of the fold, regardless of the class, as illustrated by the conservation of $C^{3.25}$ shown in Fig. 2 and S16. ECL2 is the longest extracellular loop in GCR1, and this too is a typical feature of the GPCR fold (Venkatakrishnan et al. 2013). The conserved WCW motif in ECL2 occurs in a similar position to the class B ECL2 CW motif, as shown in Fig. S17. In addition, GCR1 has a potential sodium binding site that lies between TM2, TM3 and TM7, identified by simulations (Selent et al. 2010) and crystallography (Liu et al. 2012) that is only found in class A GPCRs. The other motif that is only found in class A GPCRs is $Y^{5.58}$, that is involved in stabilizing the active GPCR conformation (White et al. 2012). GCR1 homologues share an FxxP motif on TM5 with both class A and class B GPCRs, but in class A GPCRs this is displaced by 1 turn of the helix.

Given the conserved L at position 1.63, it appears that GCR1 / class E shares the novel KKLH motif on intracellular loop 1, ICL1, albeit in a modified form, with the consensus being KELR and which interacts with a polar/hydrophobic motif on helix 8 (SVxxxI in GCR1, EFxxxF in class A and EVxxxL in class B); this motif is difficult to align (Roy et al. 2013) but came to light in ungapped inter-class helix alignments (Vohra et al. 2013). The length of the intracellular loops may also be highly relevant. In the β_2-AR – Gs complex, both ICL1 and ICL2 interact with the G protein. Analysis of the alignments in the PRINTS database shows that ICL1 is the same length in the majority of class B and GCR1 sequences while (ICL1 is the same length in 68% of PRINTS class A sequences and all but 12% have the same length to within 1 residue; ICL2 is the same length in class B and GCR1 (bar 9% of PRINTS class B sequences). In common with many GPCRs, ICL3 of GCR1 is the longest intracellular loop.

The class A EFxxxF motif is part of the ampiphilic helix 8 that runs parallel to the membrane plane, as shown by most GPCR crystal structures, the exceptions being CXCR4 (Wu et al. 2010) which has positive residues (hence a repulsive interaction at positions 1.61, 1.62 and 8.49), the neurotensin NTSR1, where the thermostabilized construct is inactive even though it is an 'active' agonist bound structure (White et al. 2012) and the class B corticotropin releasing factor receptor 1, where H8 was truncated (Hollenstein et al. 2013). The structural motif is present in class B and F GPCRs as illustrated by the glucagon (Siu et al. 2013) and the smoothened receptor (Wang et al. 2013) structures; it is therefore a structural feature characteristic of GPCRs. The signature for an

ampipathic helix 8 is strong in class B, class D, class F and plant GPCRs as can be seen from the sequence alignments at the PRINTS database (Fig. S18), The C-terminal region beyond the ampipathic helix of GCR1 is rich in serines and threonines, as could be expected by analogy to other GPCR classes, and a number of serine/threonine kinases exist in *Arabidopsis* that have homology to mamalian G protein coupled receptor kinases, However, there is less evidence for plant analogues of arrestin, which binds phosporylated GPCRs in mammalian systems and so other proteins could be involved in GCR1 internalization (Urano et al. 2013). There is a consensus glycosylation site, Nx[S/T], in ECL2. While N-glycosylation in the N-terminus is common, 32% of GPCRs have at least one glycosylation site in ECL2 and 85% of these are between the top of TM4 and the conserved Cys (Wheatley et al. 2012).

For the alignment of remote homologues, reliance solely on alignment scores and or statistics is unwise, but rather it is important to identify common motifs (Lesk 2002). In summary, a number of common motifs have been identified. Many of these reside in regions associated with receptor activation and G protein binding. These motifs are prime candidates for experiments to investigate the possibility that the similarity that GCR1 shares with its class A and class B cousins underlies an ability to interact with heterotrimeric G proteins irrespective of any GEF or other regulatory action.

The DRY motif. The two most important class A activation microswitches are DRY$^{3.51}$ on TM3 and NPXXY$^{7.53}$ on TM7. The second microswitch has readily identifiable counterparts in both class B (VAVLY$^{7.53}$) and GCR1 (NSIAY$^{7.53}$), but the DRY$^{3.51}$ motif raises difficulties, since the class B positional equivalent (YLH$^{3.51}$) is not as important in activation as its class A counterpart and the class B DRY$^{3.51}$ functional equivalent, which also involves charged residues, is disjoint as it is distributed between TM2 and TM3 (Frimurer and Bywater 1999;Vohra et al. 2013). Fig. S16 shows that contiguous charged/aromatic residues are also missing from TM3 positions 3.49 – 3.51 in class C, class D, class E, GCR1 and class F GPCRs. Consequently, in these GPCRs it is highly likely that the DRY$^{3.51}$ functionally equivalent motif may use different positions and take an alternative form that could involve polar rather than charged residues. The class A GPCR-Gs interaction is mediated by positive residues on the GPCR, most notably R$^{3.50}$, but the C-terminal peptide of Gs is not rich in negative residues. On the assumption that the DRY$^{3.51}$ functionally equivalent motif donates a hydrogen bond to the G protein, possible GCR1 candidate residues could include R107$^{3.52}$, R48$^{1.64}$ and K49$^{2.37}$, which could adopt the right conformation given minor conformational changes to intracellular loop 1 (ICL1). Of these, K49$^{2.37}$ is the most likely as it could also form an ionic lock with Glu211$^{6.30}$ in the inactive structures. However, the C-terminal part of the plant G protein (GPA1_ARATH) has 3 consecutive Arg residues (373-375) that may mediate the GPCR – G protein interaction and so the use of positive residues by class A and class B GPCRs may not be followed by other classes. In our model, S51$^{2.39}$ is the only residue in TM2 and TM3 making interactions to charged residues in the GAP1 C-terminus). Such a small polar residue would seem an unlikely alternative, but (Rosenkilde et

al. 2005) describe a constitutively active viral-encoded GPCR containing a DTW$^{3.51}$ motif. With regard to a possible ionic lock involving Glu211$^{6.30}$, Glu is not highly conserved at position 6.30 in GCR1/class E, but neither is it highly conserved in class A. Given the potential role of Thr in the class B polar lock (Vohra et al. 2013), Glu211$^{6.30}$ could also form a potential polar lock with T108$^{3.53}$.

The uncertainty in analyzing these potential interactions arises because of difficulties in modeling loops (Goldfeld et al. 2011), but this is not a major issue with regards to whether GCR1 has a GPCR-specific 7TM fold since many of the motifs listed in Tables 4 and shown in Fig. 4C reside within the helices, not the loops. While comparative models may be useful for giving an overall picture of GPCR interactions (Taddese et al. 2012;Taddese et al. 2013) they are certainly not completely reliable and so are better used for indicating possible candidate residues for mutagenesis experiments than for providing a definitive identification of all key residues. For these reasons, and because of the lack of mutagenesis data, Table 4 does not specify a GCR1/class E functional equivalent of the DRY motif or an ionic/polar lock.

Group Conserved residues

The positions of the 24 helical group-conserved residues (Eilers et al. 2005) that are common to class A, class B and GCR1/class E are given in Table S13. Each individual helix arrangement appears to be non-random with 14 of the group-conserved residues being of the same type in all 3 classes.

Alignment quality

The quality scores for the alignment between GCR1 homologues and class A or class B, and the comparative score for random sequences are given in Fig. 6. For each helix, with the possible exception of TM6 for class A, the score for the alignment between GCR1 homologues and class A, and particularly class B, is such that very few of the alternative alignments give a lower score. It appears that the distribution of entropy in each pair of aligned helices is not random and it is reassuring that similar results are obtained for each helix. However, it is not possible to extend this analysis to the whole alignment since the evolution of one helix may not be entirely independent of that of another helix.

What is the true identity of the non-GPCRs?

The fold recognition results indicate that a number of proteins, namely the MtN3 family, At2g16970 and At1g71960 are likely to be transporters; this is discussed further in supporting information.

The GPA1 - GCR1 – GEF dilema

The observation that GPA1 is self-activating in that it readily binds GTP rather than requiring a GPCR to catalyse the exchange of GDP for GTP (Johnston et al. 2007) has led to the suggestion that the activity of GPA1 is regulated by RGS (regulator of G protein signaling, a GTPase-accelerating protein) rather than by a GPCR, though some plants lack RGS (Urano et al. 2012). Hence it has been implied that GPA1 does not require a GEF and therefore that GCR1 is not a GPCR since it is not required to regulate GPA1.

In contrast, GCR1 has been shown to interact with GPA1 by both a split ubiquitin method and coimmunoprecipitation (Pandey and Assmann 2004). GCR1 was also predicted to have a GPCR fold by the fold recognition methods, and this implies much more than a collection of 7 randomly packed transmembrane helices but rather the GPCR fold implies very specific helix lengths, tilts, rotations and helix-helix interactions; the GPCR 7TM fold is usually accompanied by an 8^{th} helix. Other additional evidence that GCR1 shares the GPCR fold comes from the alignments, variability, the experimentally validated class A – class B alignment, the identification of GPCR motifs, analysis of the loop lengths and the alignment of group conserved residues. Consequently, GCR1's status as a GPCR cannot be dismissed merely because it does not behave as a GEF in current experiments. It appears then that the two contrasting observations must be held in tension until a resolution of the apparent contradiction is uncovered. This resolution may reside in the complexity of the plant signaling apparatus.

The issue as to whether GPCRs are GEFs is not new to the GPCR field. Indeed, for many years this question was used as an objection to recognizing class F Frizzled receptors as GPCRs. This objection was overturned by biochemical evidence (Malbon 2011;Koval and Katanaev 2011), and more recently by an X-ray crystal structure (Wang et al. 2013). In addition, the idea that GPA1 does not need a GEF, does not necessarily mean that GCR1 is not a GEF, even if GPA1 is the only Gα subunit in *Arabidopsis.*

Given that GCR1 has a GPCR fold, it would be interesting to see whether GCR1 behaves as a GEF in a chimeric GPA1 in which the part of the helical domain responsible for GPA1 self activation was replaced by a corresponding part from a non-self-activating G protein (Jones et al. 2011); since GCR1 may interact more readily with a GDP-bound form of GPA1, this may also help to reconcile conflicting reports as to whether GCR1 does indeed interact with GPA1 (Pandey and Assmann 2004;Urano et al. 2013).

If GCR1 was ultimately found not to couple to G proteins in any circumstances, this would be particularly interesting given that it has the features expected of a *bone fide* GPCR in terms of fold and motifs.

Decoy GPCRs

GPCRs are not always defined by their GEF activity, as GPCRs also promote G protein independent signaling with conventional signaling partners (Bockaert and Pin 1999;Rajagopal et al. 2010b;Whalen et al. 2011;Koval and Katanaev 2011). This is illustrated for example by the 'decoy' GPCRs. Decoy GPCRs have the expected GPCR motifs and are considered part of the GPCR family but do not signal through G proteins. These include C5L2 and CXCR7 (Okinaga et al. 2003;Chen et al. 2007;Rajagopal et al. 2010a). CXCR7 has all the motifs given in Table 4 except that the KKLH motif appears as KTTG, the KxxK$^{6.32}$ motif appears as SSRK and there is no obvious ionic lock). Wild type H2LC has DLC$^{3.51}$ instead of the DRY motif – but the G protein coupling is restored if this is mutated to DRC; in other respects it is a chemokine GPCR. If GCR1 does not couple to G proteins, then GCR1 could also be designated as a decoy GPCR. However, unlike CXCR7 (Rajagopal et al. 2010a), it probably does not have the option of signaling through arrestin and so it would be interesting to identify any G protein independent signaling pathways of GCR1.

Conclusions

Here we have presented a novel perspective on the likelihood that the putative plant GPCRs derived from genome analysis are genuine GPCRs using heuristic fold recognition methods. Only GCR1 emerges as a strong GPCR candidate and for ~6 other proteins (The TOM3 family, At2g01070, At5g27210 and At3g59090) there are additional indications, beyond seven transmembrane helices, that they could have a GPCR fold, but these indications are weak. For some candidate GPCRs, there is little consensus as to their true identity (~37) while for others (~10) it is more likely that they are transporters. Thus, to predict GPCRs, the identification of seven hydrophobic regions is only the first step (Urano and Jones 2013). We have shown that it is important to also consider fold and motifs e.g. as in (Krishnan et al. 2012), to distinguish between GPCRs and other proteins that may share a 7TM scaffold.

Eleven pieces of evidence are relevant to the debate as to whether GCR1 has a GPCR fold. (i) All five fold recognition methods matched GCR1 to the GPCR fold. (ii) GCR1 homologues were used as a bridge in the experimentally-validated class A – class B GPCR alignment (Vohra et al. 2013). (iii) The alignment method has been validated on the class A – class B – class F alignments. (iv) The alignments of the GCR1 homologues to class A, class B and class F GPCRs are clear and mutually consistent (ex TM6 class F). (v) The helix-helix alignments involving GCR1 homologues have a higher similarity (Fig. 4A) than the well-established class A – class B - class F GPCR alignments. (vi) Patterns of variability on all 7 helices are consistent with the GPCR fold. (vii) The alignment has identified 15 motifs that GCR1 shares with class A and class B GPCRs, including the diagnostic

disulfide bond between TM3 and ECL2. (viii) GCR1 has an ampipathic 8th helix, which is characteristic of GPCRs and which has Ser and Thr residues in the expected positions. (ix) The lengths of ICL1 and ICL2 in GCR1 are largely identical to those of their class A and or class B counterparts. (x) The lengths of ECL2 and ICL3 relative to the other loops are as expected for a GPCR. (xi) The alignment of any given individual helix appears to be non-random. Together, this evidence validates the use of GCR1 as an intermediate sequence in the class A – class B alignment.

This creates an interesting dilemma when seen against the issues of heterotrimeric G protein regulation raised by (Urano and Jones 2013), which suggest that GCR1 is not a GPCR, primarily because GPA1 and other similar G proteins in lower organisms do not need a GEF (Urano et al. 2012;Urano and Jones 2013;Urano et al. 2013;Bradford et al. 2013). Whether GCR1 is ultimately confirmed as a G protein-interacting protein, (as the Frizzled-smoothened GPCRs were after a long debate (Malbon 2011;Koval and Katanaev 2011)) remains to be seen. If it is not confirmed as a GPCR then it raises a very interesting question as to the function of a protein that has the fold and expected motifs of a bone fide GPCR. Thus, if GCR1 has a function that is not well-known for GPCRs, then other well-accepted GPCRs may possibly have similar hitherto unknown functions.

Literature Cited

Abagyan R (2013) From GPCR structure to predicted models. Presented at Drug Discovery Chemistry's inaugral GPCR-based drug design: computational and structural approaches, San Diego.

Attwood TK, Coletta A, Muirhead G, Pavlopoulou A, Philippou PB, Popov I, Roma-Mateo C, Theodosiou A, Mitchell AL (2012) The PRINTS database: a fine-grained protein sequence annotation and analysis resource--its status in 2012. Database (Oxford) **2012**: bas019

Attwood TK, Findlay JB (1994) Fingerprinting G-protein-coupled receptors. Protein Eng **7**: 195-203

Baldwin JM, Schertler GF, Unger VM (1997) An alpha-carbon template for the transmembrane helices in the rhodopsin family of G-protein-coupled receptors. J Mol Biol **272**: 144-164

Ballesteros JA, Weinstein H (1995) Integrated methods for the construction of three-dimensional models and computational probing of structure-function relationships in G-protein coupled receptors. Methods Neurosci **25**: 366-428

Bissantz C, Logean A, Rognan D (2004) High-throughput modeling of human G-protein coupled receptors: amino acid sequence alignment, three-dimensional model building, and receptor library screening. J Chem Inf Comput Sci **44**: 1162-1176

Bockaert J, Pin JP (1999) Molecular tinkering of G protein-coupled receptors: an evolutionary success. EMBO J **18**: 1723-1729

Bradford W, Buckholz A, Morton J, Price C, Jones AM, Urano D (2013) Eukaryotic g protein signaling evolved to require g protein-coupled receptors for activation. Sci Signal **6**: ra37

Chabbert M, Castel H, Pele J, Deville J, Legendre R, Rodien P (2012) Evolution of class a g-protein-coupled receptors: implications for molecular modeling. Curr Med Chem **19**: 1110-1118

Chen JG, Pandey S, Huang JR, Alonso JM, Ecker JR, Assmann SM, Jones AM (2004) GCR1 can act independently of heterotrimeric G-protein in response to brassinosteroids and gibberellins in Arabidopsis seed germination. Plant Physiology **135**: 907-915

Chen JH, Guo J, Chen JG, Nair SK (2013) Crystal structure of arabidopsis GCR2 identifies a novel clade of lanbiotic cyclase-like proteins. www rcsb org, PDB Code 3T33

Chen NJ, Mirtsos C, Suh D, Lu YC, Lin WJ, McKerlie C, Lee T, Baribault H, Tian H, Yeh WC (2007) C5L2 is critical for the biological activities of the anaphylatoxins C5a and C3a. Nature **446**: 203-207

Chien EY, Liu W, Zhao Q, Katritch V, Han GW, Hanson MA, Shi L, Newman AH, Javitch JA, Cherezov V, Stevens RC (2010) Structure of the human dopamine D3 receptor in complex with a D2/D3 selective antagonist. Science **330**: 1091-1095

Clamp M, Cuff J, Searle SM, Barton GJ (2004) The Jalview Java alignment editor. Bioinformatics **20**: 426-427

Claros MG, Von HG (1994) TopPred II: an improved software for membrane protein structure predictions. Comput Appl Biosci **10**: 685-686

Congreve M, Langmead CJ, Mason JS, Marshall FH (2011) Progress in structure based drug design for G protein-coupled receptors. J Med Chem **54**: 4283-4311

Coopman K, Wallis R, Robb G, Brown AJ, Wilkinson GF, Timms D, Willars GB (2011) Residues within the transmembrane domain of the glucagon-like peptide-1 receptor involved in ligand binding and receptor activation: modelling the ligand-bound receptor. Mol Endocrinol **25**: 1804-1818

Dong M, Lam PC, Gao F, Hosohata K, Pinon DI, Sexton PM, Abagyan R, Miller LJ (2007) Molecular approximations between residues 21 and 23 of secretin and its receptor: development of a model for peptide docking with the amino terminus of the secretin receptor. Mol Pharmacol **72**: 280-290

Doolittle RF (1986) Of URFs and ORFs: a primer on how to analyze derived amino acid sequences. University Science Books, Mill Valley California,

Eilers M, Hornak V, Smith SO, Konopka JB (2005) Comparison of class A and D G protein-coupled receptors: common features in structure and activation. Biochemistry **44**: 8959-8975

Eswar N, Webb B, Marti-Renom MA, Madhusudhan MS, Eramian D, Shen MY, Pieper U, Sali A (2006) Comparative protein structure modeling using Modeller. Curr Protoc Bioinformatics **Chapter 5**: Unit

Fredriksson R, Lagerstrom MC, Lundin LG, Schioth HB (2003) The G-protein-coupled receptors in the human genome form five main families. Phylogenetic analysis, paralogon groups, and fingerprints. Mol Pharmacol **63**: 1256-1272

Frimurer TM, Bywater RP (1999) Structure of the integral membrane domain of the GLP1 receptor. Proteins **35**: 375-386

Goldfeld DA, Zhu K, Beuming T, Friesner RA (2011) Successful prediction of the intra- and extracellular loops of four G-protein-coupled receptors. Proc Natl Acad Sci U S A **108**: 8275-8280

Gookin TE, Kim J, Assmann SM (2008) Whole proteome identification of plant candidate G-protein coupled receptors in Arabidopsis, rice, and poplar: computational prediction and in-vivo protein coupling. Genome Biol **9**: R120

Gregory KJ, Nguyen ED, Reiff SD, Squire EF, Stauffer SR, Lindsley CW, Meiler J, Conn PJ (2013) Probing the metabotropic glutamate receptor 5 (mGlu(5)) positive allosteric modulator (PAM) binding pocket: discovery of point mutations that engender a "molecular switch" in PAM pharmacology. Mol Pharmacol **83**: 991-1006

Haga K, Kruse AC, Asada H, Yurugi-Kobayashi T, Shiroishi M, Zhang C, Weis WI, Okada T, Kobilka BK, Haga T, Kobayashi T (2012) Structure of the human M2 muscarinic acetylcholine receptor bound to an antagonist. Nature **482**: 547-551

Hanson MA, Roth CB, Jo E, Griffith MT, Scott FL, Reinhart G, Desale H, Clemons B, Cahalan SM, Schuerer SC, Sanna MG, Han GW, Kuhn P, Rosen H, Stevens RC (2012) Crystal structure of a lipid G protein-coupled receptor. Science **335**: 851-855

Henikoff S, Henikoff JG (1993) Performance evaluation of amino acid substitution matrices. Proteins **17**: 49-61

Hibert MF, Trumpp-Kallmeyer S, Hoflack J, Bruinvels A (1993) This is not a G protein-coupled receptor. Trends Pharmacol Sci **14**: 7-12

Hoflack J, Trumpp-Kallmeyer S, Hibert M (1994) Re-evaluation of bacteriorhodopsin as a model for G protein-coupled receptors. Trends Pharmacol Sci **15**: 7-9

Hollenstein K, Kean J, Bortolato A, Cheng RK, Dore AS, Jazayeri A, Cooke RM, Weir M, Marshall FH (2013) Structure of class B GPCR corticotropin-releasing factor receptor 1. Nature **499**: 438-443

Hooley R (1999) A role for G proteins in plant hormone signalling? Plant Physiology and Biochemistry **37**: 393-402

Horn F, Bettler E, Oliveira L, Campagne F, Cohen FE, Vriend G (2003) GPCRDB information system for G protein-coupled receptors. Nucleic Acids Res **31**: 294-297

Humphrey W, Dalke A, Schulten K (1996) VMD: visual molecular dynamics. J Mol Graph **14**: 33-38

Illingworth CJ, Parkes KE, Snell CR, Mullineaux PM, Reynolds CA (2008) Criteria for confirming sequence periodicity identified by Fourier transform analysis: application to GCR2, a candidate plant GPCR? Biophys Chem **133**: 28-35

Inoue Y, Yamazaki Y, Shimizu T (2005) How accurately can we discriminate G-protein-coupled receptors as 7-tms TM protein sequences from other sequences? Biochemical and Biophysical Research Communications **338**: 1542-1546

Jaakola VP, Griffith MT, Hanson MA, Cherezov V, Chien EY, Lane JR, Ijzerman AP, Stevens RC (2008) The 2.6 angstrom crystal structure of a human A2A adenosine receptor bound to an antagonist. Science **322**: 1211-1217

Janetopoulos C, Jin T, Devreotes P (2001) Receptor-mediated activation of heterotrimeric G-proteins in living cells. Science **291**: 2408-2411

Johnston CA, Taylor JP, Gao Y, Kimple AJ, Grigston JC, Chen JG, Siderovski DP, Jones AM, Willard FS (2007) GTPase acceleration as the rate-limiting step in Arabidopsis G protein-coupled sugar signaling. Proc Natl Acad Sci U S A **104**: 17317-17322

Johnston CA, Willard MD, Kimple AJ, Siderovski DP, Willard FS (2008) A sweet cycle for Arabidopsis G-proteins: Recent discoveries and controversies in plant G-protein signal transduction. Plant Signal Behav **3**: 1067-1076

Jones DT (1998) THREADER: protein sequence threading by double dynamic programming. In SL Salzberg, DB Searls, S Kasif, eds, Computational methods in Molecular Biology. Elsevier, Amsterdam, pp 285-311

Jones DT (1999a) GenTHREADER: an efficient and reliable protein fold recognition method for genomic sequences. J Mol Biol **287**: 797-815

Jones DT (1999b) Protein secondary structure prediction based on position-specific scoring matrices. J Mol Biol **292**: 195-202

Jones DT (2007) Improving the accuracy of transmembrane protein topology prediction using evolutionary information. Bioinformatics **23**: 538-544

Jones DT, Taylor WR, Thornton JM (1992) A new approach to protein fold recognition. Nature **358**: 86-89

Jones DT, Taylor WR, Thornton JM (1994) A model recognition approach to the prediction of all-helical membrane protein structure and topology. Biochemistry **33**: 3038-3049

Jones JC, Duffy JW, Machius M, Temple BR, Dohlman HG, Jones AM (2011) The crystal structure of a self-activating G protein alpha subunit reveals its distinct mechanism of signal initiation. Sci Signal **4**: ra8

Josefsson LG, Rask L (1997) Cloning of a putative G-protein-coupled receptor from Arabidopsis thaliana. Eur J Biochem **249**: 415-420

Kahsay RY, Gao G, Liao L (2005) An improved hidden Markov model for transmembrane protein detection and topology prediction and its applications to complete genomes. Bioinformatics **21**: 1853-1858

Kanehisa M, Goto S (2000) KEGG: kyoto encyclopedia of genes and genomes. Nucleic Acids Res **28**: 27-30

Kanehisa M, Goto S, Furumichi M, Tanabe M, Hirakawa M (2010) KEGG for representation and analysis of molecular networks involving diseases and drugs. Nucleic Acids Res **38**: D355-D360

Kanehisa M, Goto S, Hattori M, oki-Kinoshita KF, Itoh M, Kawashima S, Katayama T, Araki M, Hirakawa M (2006) From genomics to chemical genomics: new developments in KEGG. Nucleic Acids Res **34**: D354-D357

Katritch V, Cherezov V, Stevens RC (2013) Structure-function of the G protein-coupled receptor family. Annu Rev Pharmacol Toxicol **53**: 531-556

Kolakowski LF, Jr. (1994) GCRDb: a G-protein-coupled receptor database. Receptors Channels **2**: 1-7

Koval A, Katanaev VL (2011) Wnt3a stimulation elicits G-protein-coupled receptor properties of mammalian Frizzled proteins. Biochem J **433**: 435-440

Kratochwil NA, Malherbe P, Lindemann L, Ebeling M, Hoener MC, Muhlemann A, Porter RH, Stahl M, Gerber PR (2005) An automated system for the analysis of G protein-coupled receptor transmembrane binding pockets: alignment, receptor-based pharmacophores, and their application. J Chem Inf Model **45**: 1324-1336

Krishnan A, Almen MS, Fredriksson R, Schioth HB (2012) The Origin of GPCRs: Identification of Mammalian like Rhodopsin, Adhesion, Glutamate and Frizzled GPCRs in Fungi. PLoS One **7**: e29817

Krogh A, Larsson B, von HG, Sonnhammer EL (2001) Predicting transmembrane protein topology with a hidden Markov model: application to complete genomes. J Mol Biol **305**: 567-580

Lagerstrom MC, Schioth HB (2008) Structural diversity of G protein-coupled receptors and significance for drug discovery. Nat Rev Drug Discov **7**: 339-357

Lesk AM (2002) Introduction to Bioinformatics. OUP, Oxford,

Liu W, Chun E, Thompson AA, Chubukov P, Xu F, Katritch V, Han GW, Roth CB, Heitman LH, Ijzerman AP, Cherezov V, Stevens RC (2012) Structural basis for allosteric regulation of GPCRs by sodium ions. Science **337**: 232-236

Liu XG, Yue YL, Li B, Nie YL, Li W, Wu WH, Ma LG (2007) A G protein-coupled receptor is a plasma membrane receptor for the plant hormone abscisic acid. Science **315**: 1712-1716

Malbon CC (2011) Wnt signalling: the case of the 'missing' G-protein. Biochem J **433**: e3-e5

McGuffin LJ, Jones DT (2003) Improvement of the GenTHREADER method for genomic fold recognition. Bioinformatics **19**: 874-881

Melen K, Krogh A, von Heijne G (2003) Reliability measures for membrane protein topology prediction algorithms. Journal of Molecular Biology **327**: 735-744

Miedlich SU, Gama L, Seuwen K, Wolf RM, Breitwieser GE (2004) Homology modeling of the transmembrane domain of the human calcium sensing receptor and localization of an allosteric binding site. J Biol Chem **279**: 7254-7263

Moller S, Croning MD, Apweiler R (2001) Evaluation of methods for the prediction of membrane spanning regions. Bioinformatics **17**: 646-653

Moriyama EN, Strope PK, Opiyo SO, Chen Z, Jones AM (2006) Mining the Arabidopsis thaliana genome for highly-divergent seven transmembrane receptors. Genome Biol **7**: R96

Moult J, Fidelis K, Kryshtafovych A, Rost B, Tramontano A (2009) Critical assessment of methods of protein structure prediction - Round VIII. Proteins **77 Suppl 9**: 1-4

nett-Lovsey RM, Herbert AD, Sternberg MJ, Kelley LA (2008) Exploring the extremes of sequence/structure space with ensemble fold recognition in the program Phyre. Proteins **70**: 611-625

Ng PC, Henikoff JG, Henikoff S (2000) PHAT: a transmembrane-specific substitution matrix. Predicted hydrophobic and transmembrane. Bioinformatics **16**: 760-766

Okinaga S, Slattery D, Humbles A, Zsengeller Z, Morteau O, Kinrade MB, Brodbeck RM, Krause JE, Choe HR, Gerard NP, Gerard C (2003) C5L2, a nonsignaling C5A binding protein. Biochemistry **42**: 9406-9415

Palczewski K, Kumasaka T, Hori T, Behnke CA, Motoshima H, Fox BA, Le T, I, Teller DC, Okada T, Stenkamp RE, Yamamoto M, Miyano M (2000) Crystal structure of rhodopsin: A G protein-coupled receptor. Science **289**: 739-745

Pandey S, Assmann SM (2004) The Arabidopsis putative G protein-coupled receptor GCR1 interacts with the G protein alpha subunit GPA1 and regulates abscisic acid signaling. Plant Cell **16**: 1616-1632

Pandey S, Nelson DC, Assmann SM (2009) Two novel GPCR-type G proteins are abscisic acid receptors in Arabidopsis. Cell **136**: 136-148

Plakidou-Dymock S, Dymock D, Hooley R (1998) A higher plant seven-transmembrane receptor that influences sensitivity to cytokinins. Curr Biol **8**: 315-324

Rajagopal S, Kim J, Ahn S, Craig S, Lam CM, Gerard NP, Gerard C, Lefkowitz RJ (2010a) Beta-arrestin- but not G protein-mediated signaling by the "decoy" receptor CXCR7. Proc Natl Acad Sci U S A **107**: 628-632

Rajagopal S, Rajagopal K, Lefkowitz RJ (2010b) Teaching old receptors new tricks: biasing seven-transmembrane receptors. Nat Rev Drug Discov **9**: 373-386

Ray S, Chen Y, Ayoung J, Hanna R, Brazill D (2011) Phospholipase D controls Dictyostelium development by regulating G protein signaling. Cell Signal **23**: 335-343

Rosenkilde MM, Kledal TN, Schwartz TW (2005) High constitutive activity of a virus-encoded seven transmembrane receptor in the absence of the conserved DRY motif (Asp-Arg-Tyr) in transmembrane helix 3. Mol Pharmacol **68**: 11-19

Roy A, Kucukural A, Zhang Y (2010) I-TASSER: a unified platform for automated protein structure and function prediction. Nat Protoc **5**: 725-738

Roy A, Taddese B, Vohra S, Thimmaraju PK, Illingworth CJ, Simpson LM, Mukherjee K, Reynolds CA, Chintapalli SV (2013) Identifying subset errors in multiple sequence alignments. J Biomol Struct Dyn DOI:10 1080/073911022013 77037

Sandberg M, Eriksson L, Jonsson J, Sjostrom M, Wold S (1998) New chemical descriptors relevant for the design of biologically active peptides. A multivariate characterization of 87 amino acids. J Med Chem **41**: 2481-2491

Selent J, Sanz F, Pastor M, De FG (2010) Induced effects of sodium ions on dopaminergic G-protein coupled receptors. PLoS Comput Biol **6**: e1000884

Sheikh SP, Vilardarga JP, Baranski TJ, Lichtarge O, Iiri T, Meng EC, Nissenson RA, Bourne HR (1999) Similar structures and shared switch mechanisms of the beta2-adrenoceptor and the parathyroid hormone receptor. Zn(II) bridges between helices III and VI block activation. J Biol Chem **274**: 17033-17041

Shi J, Blundell TL, Mizuguchi K (2001) FUGUE: sequence-structure homology recognition using environment-specific substitution tables and structure-dependent gap penalties. J Mol Biol **310**: 243-257

Shimamura T, Shiroishi M, Weyand S, Tsujimoto H, Winter G, Katritch V, Abagyan R, Cherezov V, Liu W, Han GW, Kobayashi T, Stevens RC, Iwata S (2011) Structure of the human histamine H1 receptor complex with doxepin. Nature **475**: 65-70

Siu FY, He M, de GC, Han GW, Yang D, Zhang Z, Zhou C, Xu Q, Wacker D, Joseph JS, Liu W, Lau J, Cherezov V, Katritch V, Wang MW, Stevens RC (2013) Structure of the human glucagon class B G-protein-coupled receptor. Nature **499**: 444-449

Soding J, Biegert A, Lupas AN (2005) The HHpred interactive server for protein homology detection and structure prediction. Nucleic Acids Res **33**: W244-W248

Stamm M, Staritzbichler R, Khafizov K, Forrest LR (2013) Alignment of helical membrane protein sequences using AlignMe. PLoS One **8**: e57731

Styczynski MP, Jensen KL, Rigoutsos I, Stephanopoulos G (2008) BLOSUM62 miscalculations improve search performance. Nat Biotechnol **26**: 274-275

Taddese B, Simpson LM, Wall ID, Blaney FE, Kidley NJ, Clark HS, Smith RE, Upton GJ, Gouldson PR, Psaroudakis G, Bywater RP, Reynolds CA (2012) G-protein-coupled receptor dynamics: dimerization and activation models compared with experiment. Biochem Soc Trans **40**: 394-399

Taddese B, Simpson LM, Wall ID, Blaney FE, Reynolds CA (2013) Modeling active GPCR conformations. Methods Enzymol **522**: 21-35

Tusnady GE, Simon I (1998) Principles governing amino acid composition of integral membrane proteins: application to topology prediction. J Mol Biol **283**: 489-506

Tusnady GE, Simon I (2001) The HMMTOP transmembrane topology prediction server. Bioinformatics **17**: 849-850

Urano D, Chen JG, Botella JR, Jones AM (2013) Heterotrimeric G protein signalling in the plant kingdom. Open Biol **3**: 120186

Urano D, Jones AM (2013) "Round up the usual suspects": a comment on nonexistent plant g protein-coupled receptors. Plant Physiol **161**: 1097-1102

Urano D, Jones JC, Wang H, Matthews M, Bradford W, Bennetzen JL, Jones AM (2012) G protein activation without a GEF in the plant kingdom. PLoS Genet **8**: e1002756

Venkatakrishnan AJ, Deupi X, Lebon G, Tate CG, Schertler GF, Babu MM (2013) Molecular signatures of G-protein-coupled receptors. Nature **494**: 185-194

Viklund H, Bernsel A, Skwark M, Elofsson A (2008) SPOCTOPUS: a combined predictor of signal peptides and membrane protein topology. Bioinformatics **24**: 2928-2929

Viklund H, Elofsson A (2008) OCTOPUS: improving topology prediction by two-track ANN-based preference scores and an extended topological grammar. Bioinformatics **24**: 1662-1668

Viklund H, Granseth E, Elofsson A (2006) Structural classification and prediction of reentrant regions in alpha-helical transmembrane proteins: application to complete genomes. J Mol Biol **361**: 591-603

Vohra S, Chintapalli SV, Illingworth CJ, Reeves PJ, Mullineaux PM, Clark HS, Dean MK, Upton GJ, Reynolds CA (2007) Computational studies of Family A and Family B GPCRs. Biochem Soc Trans **35**: 749-754

Vohra S, Taddese B, Conner AC, Poyner DR, Hay DL, Barwell J, Reeves PJ, Upton GJ, Reynolds CA (2013) Similarity between class A and class B G-protein-coupled receptors exemplified through calcitonin gene-related peptide receptor modelling and mutagenesis studies. J R Soc Interface **10**: 20120846

Vroling B, Sanders M, Baakman C, Borrmann A, Verhoeven S, Klomp J, Oliveira L, de VJ, Vriend G (2011) GPCRDB: information system for G protein-coupled receptors. Nucleic Acids Res **39**: D309-D319

Wang C, Wu H, Katritch V, Han GW, Huang XP, Liu W, Siu FY, Roth BL, Cherezov V, Stevens RC (2013) Structure of the human smoothened receptor bound to an antitumour agent. Nature **497**: 338-343

Warne T, Serrano-Vega MJ, Baker JG, Moukhametzianov R, Edwards PC, Henderson R, Leslie AG, Tate CG, Schertler GF (2008) Structure of a beta1-adrenergic G-protein-coupled receptor. Nature **454**: 486-491

Whalen EJ, Rajagopal S, Lefkowitz RJ (2011) Therapeutic potential of beta-arrestin- and G protein-biased agonists. Trends Mol Med **17**: 126-139

Wheatley M, Wootten D, Conner M, Simms J, Kendrick R, Logan R, Poyner D, Barwell J (2012) Lifting The Lid On G-Protein-Coupled Receptors: The Role Of Extracellular Loops. Br J Pharmacol **165**: 1688-1703

White JF, Noinaj N, Shibata Y, Love J, Kloss B, Xu F, Gvozdenovic-Jeremic J, Shah P, Shiloach J, Tate CG, Grisshammer R (2012) Structure of the agonist-bound neurotensin receptor. Nature **490**: 508-513

Williams JG, Noegel AA, Eichinger L (2005) Manifestations of multicellularity: Dictyostelium reports in. Trends Genet **21**: 392-398

Woolley M, Watkins HA, Taddese B, Karakullukcu ZG, Barwell J, Smith KJ, Hay DL, Poyner DR, Reynolds CA, Conner AC (2013) The role of ECL2 in CGRP receptor activation: a combined modelling and experimental approach. J Roy Soc Interface **10**: 20130589

Wu B, Chien EY, Mol CD, Fenalti G, Liu W, Katritch V, Abagyan R, Brooun A, Wells P, Bi FC, Hamel DJ, Kuhn P, Handel TM, Cherezov V, Stevens RC (2010) Structures of the CXCR4 chemokine GPCR with small-molecule and cyclic peptide antagonists. Science **330**: 1066-1071

Wu S, Zhang Y (2007) LOMETS: a local meta-threading-server for protein structure prediction. Nucleic Acids Res **35**: 3375-3382

Wu S, Zhang Y (2008) MUSTER: Improving protein sequence profile-profile alignments by using multiple sources of structure information. Proteins **72**: 547-556

Yan J, Mihaylov V, Xu X, Brzostowski JA, Li H, Liu L, Veenstra TD, Parent CA, Jin T (2012) A Gbetagamma effector, ElmoE, transduces GPCR signaling to the actin network during chemotaxis. Dev Cell **22**: 92-103

Zhang C, Srinivasan Y, Arlow DH, Fung JJ, Palmer D, Zheng Y, Green HF, Pandey A, Dror RO, Shaw DE, Weis WI, Coughlin SR, Kobilka BK (2012) High-resolution crystal structure of human protease-activated receptor 1. Nature **492**: 387-392

Zhang Y (2008) I-TASSER server for protein 3D structure prediction. BMC Bioinformatics **9**: 40

Figure Legends

Fig. 1. Various alignment results to illustrate the method; each legend is valid until replaced by an alternative. (A - C) The number of votes for each of the 17 alternative class A – class B pairwise alignments evaluated using the PHAT matrix (P, red, left) and the Blosum62 matrix (B, orange, right): (A) TM3, (B) TM1 and (C) TM7. (D) The number of votes for the TM1 class A – class B pairwise alignments evaluated using hydrophobicity (H, green, left) and volume matrix (Vo, yellow, right). (E) The maximum lagged correlation R values for each alignment evaluated using entropy (S, purple, left) and variability (Va, cyan, right) for the class A – class B TM1 alignment. (F) the R values of (E) scaled between 0 and 1.0 for the class B– class F TM2 alignment. (G) The product scores for each of the TM3 class A – class B alignments. The product scores are (left to right) (i) P × H × Vo × S (red), (ii) P × Vo × S (green), (iii) P × H × S (yellow), (iv) P × H × Vo (white) and (v) P × H × Vo × Va (purple). (H) The product scores for each of the TM5 class A – class B alignments. The product scores are (i) B × H × Vo × S (orange), (ii) B × Vo × S (green), (iii) B × H × S (yellow), (iv) B × H × Vo (white) and (v) B × H × Vo × Va (purple).

Fig. 2. The sequence alignment between GCR1 and the class A, class B and class F template sequences; the color reflects the biophysical properties. The most conserved positions within each helix in class A are marked by a vertical bar (|) and correspond to position 50. The residues are color coded according to their properties as follows: blue, positive; red, negative or small polar; purple, polar; aromatic; green large hydrophobic; yellow, small hydrophobic, cyan, polar. This corresponds to the 'Taylor' scheme, as implemented in Jalview (Clamp et al. 2004). For clarity some ungapped sequence sections have been truncated.

Fig. 3. The product of the 4 scaled scores (PHAT matrix score × hydrophobicity × volume × entropy), for the alignment between class A – GCR1 homologues (left, purple) and class B GCR1 homologues (right, cyan). The alignment corresponding to the zero alignment is given in Fig. 2. The legend given for TM1 is valid for all plots.

Fig. 4. (A) The mean percentage identity (%ID) between different GPCR families. The class A – class B, class A – class F and class B – class F %IDs are shown to the left of the vertical line in red, orange

and yellow respectively; the %IDs between class A, class B and class F with the GCR1 homologues are shown to the right in purple, blue and cyan respectively. The %IDs for TM3 between GCR1 homologues and class C and D GPCRs are 14.3% and 11.9% respectively. (B) The structural alignment (determined by Modeller using all residues) between the inactive GCR1 (green), the class A dopamine D3 (purple), the class B glucagon (blue) and the class F smoothened (cyan) receptors looking towards TM1 – TM4. The RMSD between minimized inactive GCR1 and the dopamine, glucagon and smoothened receptors is 1.29 Å, 2.07 Å and 3.33 Å respectively. For comparison, the expected RMSDs between the α, β, χ and δ class A GPCRs is 2.2 – 3.0 Å, that between class A and B GPCRs is typically 2.7 – 3.3 Å (Hollenstein et al. 2013;Siu et al. 2013) and so these RMSD are of the expected magnitude. The RMSDs were calculated over the helical domain over the range 1.36-1.59, 2.40-2.58, 3.25-3.51, 4.45-4.62, 5.43-5.65, 6.33 – 6.43 and 7.43-7.53; shorter sections were used for TM6 and TM7 because of the known outward tilt in class B in this region. (C) Snake diagram showing GCR1 features that characterize the GPCR fold. The two Cys residues of the TM3 – ECL2 disulfide bond are shown in yellow with black lettering. Motifs shared with class A and or B GPCRs are shown in red with white lettering. Group conserved residues that have the same character in class A, B and GCR1 homologues are shown in cyan with dark blue lettering; other common group conserved positions are shown in dark blue with cyan lettering. The TLH positional equivalent of the DRY motif is shown in orange (residues are only shown in one category). ICL1 and ICL2 are denoted in purple as they are the same length as their class A and or class B counterparts. ECL2 and ICL3 are shown in light blue as they are the longest ECL and ICL respectively. The amipathic helix 8 is denoted by a light green background. Potential phosphorylation sites C-terminal of the ampipathic helix are denoted by red lettering. The potential glycosylation site in ECL2 is also denoted by red lettering.

Fig. 5. Variability for each of the 7 transmembrane helices. The variability for class A GPCRs (A, solid), and class B GPCRs (B, dotted) is shown in black; the variability for GCR1 homologues is shown in orange respectively. Shading indicates the internal or buried positions (which should have low variability) For TM1, TM5 and TM6 the variability for the alternative +3, +4 and -6 GCR1 alignments (G') is shown with orange dashes. Position 7.34 is a restricted external position in many receptors, hence its low variability. The different helix lengths shown reflect both the natural helix length and the length over which a common conformation can be expected (Vohra et al. 2013). Although positions 3.35 – 3.40 in TM3 are nominally internal, they still show a maximum variability in line with the helix periodicity.

Fig. 6. A helix by helix quality assessment of the alignment of GCR1 homologues. The score from equation (1) for the alignment between GCR1 homologues and class A and class B GPCRs is denoted by lower (red) and upper (blue) arrows denoted (A:G) and (B:G) respectively. A histogram of the scores from equation (1) between GCR1 homologues and the 198 comparator sequences is also given; the number of comparator scores that are higher than the class A or class B scores are shown in parentheses beside the respective arrow.

Table 1. Threading results of putative plant GPCRs split into families of proteins that share discernable homology. Putative plant GPCRs with GPCR hit are denoted ✓; no GPCR hits are denoted ×. Each hit has an associated interpretation such as 'high', 'medium' or 'low', to indicate the expected reliability. Proteins predicted not to be 7TM proteins are underlined and the expected number of TM helices given. Non-plant 7TM lung receptors are shown in *italics*.

TAIR locus ID	I-TASSER	LOMETS	HHpred	FUGUE	Phyre
Nodulin MtN3 family proteins (8/17; 2 hits/8 proteins)					
At3g28007	×	×	×	✓ (guess)	×
At4g25010	×	×	✓ (guess)	×	×
Expressed protein family 2 (1 hit / 3 proteins)					
At2g47115	×	×	✓(uncertain)	×	×
Expressed protein family 3 (1 hit / 2 proteins)					
At5g42090	×	×	✓ (guess)	×	×
TOM3 family proteins					
At1g14530	×	×	✓ (marginal)	×	×
At2g02180	×	×	✓ (guess)	×	×
At4g21790	×	×	✓ (marginal guess)	✓ (guess)	×
Lung_7-TM_R					
At2g01070	×	✓ (high)	✓ (guess)	×	✓ (high)
Q22938_CAEEL	*✓(high)*	×	*✓(high)*	×	×
A8K285_HUMAN	×	×	*✓(guess)*	×	×
YHB7_YEAST	×	✓ (marginal)	✓ (high)	×	×

The following MtN3 proteins had no hits: At1g21460, At3g16690, At3g48740, At5g13170. The following Expressed protein family 2 proteins had no hits: At1g10660, At5g62960. The following Expressed protein family 3 protein had no hits: At3g09570. All of the Expressed protein family 5 protein had no hits: At3g63310, At4g02690. All of the GNS1/SUR4 membrane family proteins had no hits: At1g75000, At3g06470, At4g36830. All of the MLO family proteins had no hits: At1g11000, At1g26700, At1g24560, At2g33670, At2g44110, At4g24250, At5g53760. Both of the GTG family proteins had no hits: GTG1(9TM), GTG2(9TM). The groups are those reported by (Moriyama et al. 2006)

Table 2. Threading results of putative plant GPCRs split into groups of proteins that do not share discernible homology. Putative plant GPCRs with GPCR hit are indicated with ✓; no GPCR hits are indicated by × . Each hit has an associated interpretation such as 'high', 'medium' or 'low', to indicate the expected reliability. Proteins predicted not to be 7TM proteins are underlined and the expected number of TM helices given.

TAIR locus ID	I-TASSER	LOME	HHpred	FUGUE	Phyre
Misc. Single copy genes					
At1g48270(GCR1)	✓ (high)	✓ (high)	✓ (high)	✓ (high)	✓ (high)
At3g59090	×	×	×	✓ (marginal)	×
At4g20310 (4TM)	×	×	×	✓ (guess)	×
Misc. Single member from small gene families (8)					
At5g27210	×	×	×	✓ (guess)	×

There were no hits for all of the Expressed protein family 1 (fAt1g77220, At4g21570), Misc. Expressed protein family 4 (At1g49470, At5g19870), Perl1-like family protein (At1g16560, At5g62130) and the Misc. Single member from big gene families (At1g71960, At3g01550, At5g23990, At5g37310 (predicted ~9TM)). There were no hits for the following members of Misc. Single copy genes: At1g57680, At2g41610, At2g31440, At3g04970 (predicted 6TM) and At3g26090 (RGS1). There were no hits for the following members of Misc. Single member from small gene families: At3g19260, At2g35710 (predicted 6TM), At2g16970 (predicted 12TM), At1g15620 (predicted 5/6TM), At1g63110 and At4g36850.

Table 3: The 5 most likely plant GPCRs ranked according to the strength of evidence from fold recognition, sequence comparison and transmembrane helix prediction. The first rank, GCR1, is clearly a GPCR. At2g01070 and TOM3 are possibly GPCRs on the basis of more than one piece of evidence. The remaining two hits have been implicated by just one piece of evidence.

Rank	TAIR locus ID/Family
1	At1g48270(GCR1)
2	TOM3
	At2g01070
3	At5g27210
	At3g59090

Table 4 Key motifs conserved in Class A, class B and GCR1/class E GPCRs. Lowercase indicates that the GCR1 residues are not conserved.

TM	Class A motifs	Class B motifs	GCR1 motif	GCR1/class E family motifs	Probable Function (where known)
IL1	$K^{1.61}$ KLHxxxN	$R^{1.61}$KLHxxxN	KELRkfsF	$K^{1.61}$ELRxxx[F/N]	stability
TM2	NLxxx$D^{2.50}$	NLxxx$F^{2.50}$	YLalsD$^{2.50}$	YLxxx$D^{2.50}$	structure
TM2-7	$D^{2.50}$, $S^{3.39}$, $W^{6.48}$, $N^{7.45}$, $S^{7.46}$	-	$D^{2.50}$, $S^{3.39}$, $W^{6.48}$	$D^{2.50}$, [S/D]$^{3.39}$, $W^{6.48}$	Sodium binding site
TM3	$CK^{3.26}$	$CK^{3.26}$	CY	$CY^{3.26}$	Structure: disulfide bond to ECL2
DRY motif	D/E $R^{3.50}$ Y/W	$R^{2.39}$…$H^{2.43}$…$E^{3.46}$	a	a	activation
TM3	$DR^{3.50}$Y	$YL^{3.50}$H	TLH	$TL^{3.50}$[Y/H]	activation
TM4	$W^{4.50}$	$W^{4.50}$	W	$W^{4.50}$	structure
ECL2		CW	WCW	WCW	
TM5	FxxP$^{5.50}$	FxxP$^{5.46}$	FxxP$^{5.46}$	FxxP$^{5.46}$	structure
TM5	$Y^{5.58}$	-	$Y^{5.58}$	$Y^{5.58}$	activation
TM5	IxxL$^{5.65}$	IXXL$^{5.65}$	VXXI$^{5.65}$	VXXL$^{5.65}$	activation
TM6	KxxK$^{6.35}$	KxxK$^{6.35}$	KvlN	Kxx[K/N]$^{6.35}$	Activation
TM6	CWxP$^{6.50}$	$P^{6.42}$…TY$^{6.48}$	P$^{6.41}$...SWaF	P$^{6.41}$...W$^{6.48}$x[F/P]	Activation
	$R^{3.50}$, $E^{6.30}$	$R^{2.39}$, $T^{6.37}$	*a*	a	Ionic lock
TM7	NP$^{7.50}$ xxY	VA$^{7.50}$ VLY	NS$^{7.50}$ xxY	NS$^{7.50}$ xxY	activation
H8	EF$^{8.50}$xxxL	EV$^{8.50}$xxxL	SV$^{8.50}$xxxI	SV$^{8.50}$xxxI	stability

[a]See text

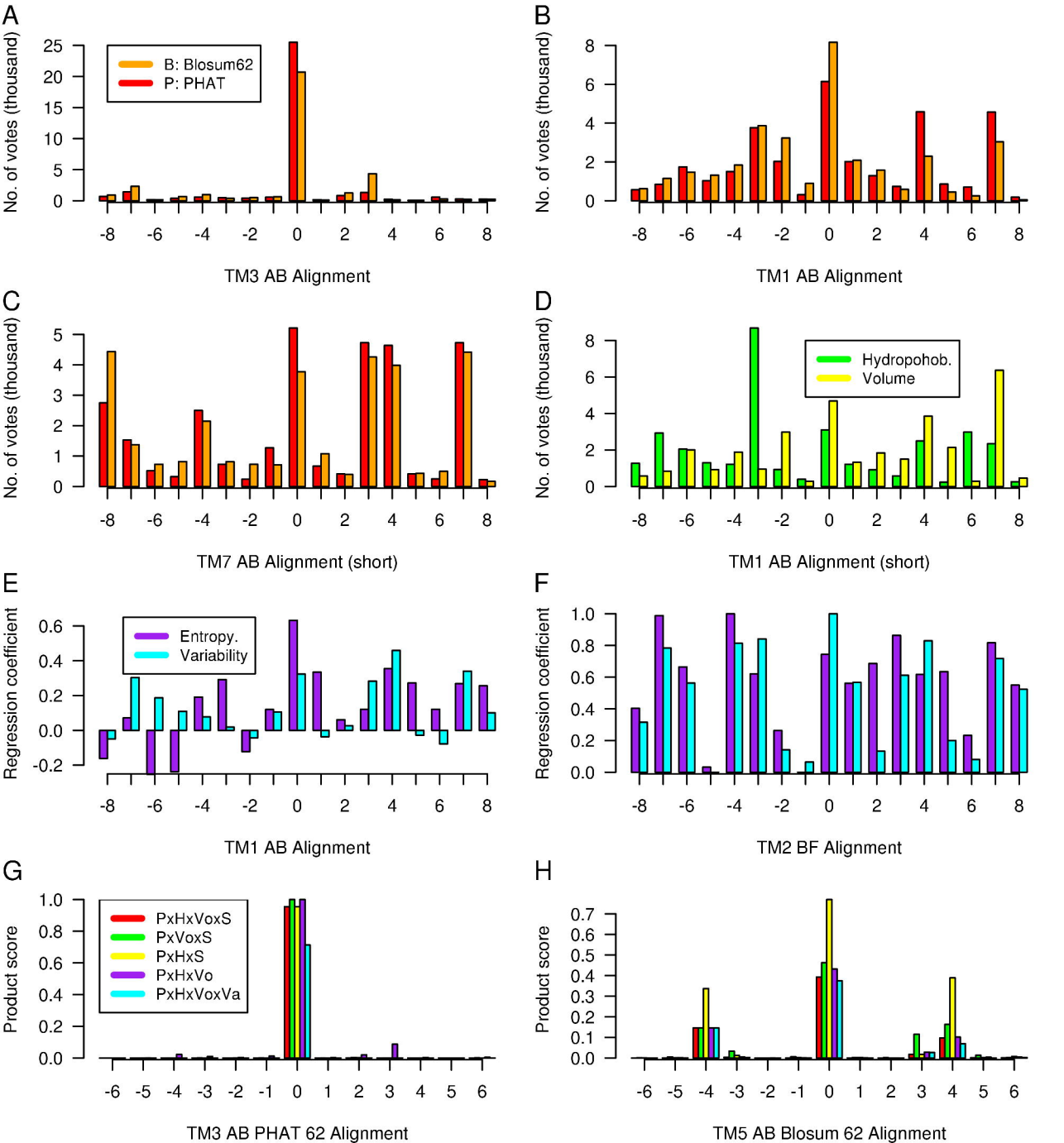
A
No. of votes (thousand)
B: Blosum62
P: PHAT
TM3 AB Alignment
B
No. of votes (thousand)
TM1 AB Alignment
C
No. of votes (thousand)
TM7 AB Alignment (short)
D
No. of votes (thousand)
Hydropohob.
Volume
TM1 AB Alignment (short)
E
Regression coefficient
Entropy.
Variability
TM1 AB Alignment
F
Regression coefficient
TM2 BF Alignment
G
Product score
PxHxVoxS
PxVoxS
PxHxS
PxHxVo
PxHxVoxVa
TM3 AB PHAT 62 Alignment
H
Product score
TM5 AB Blosum 62 Alignment

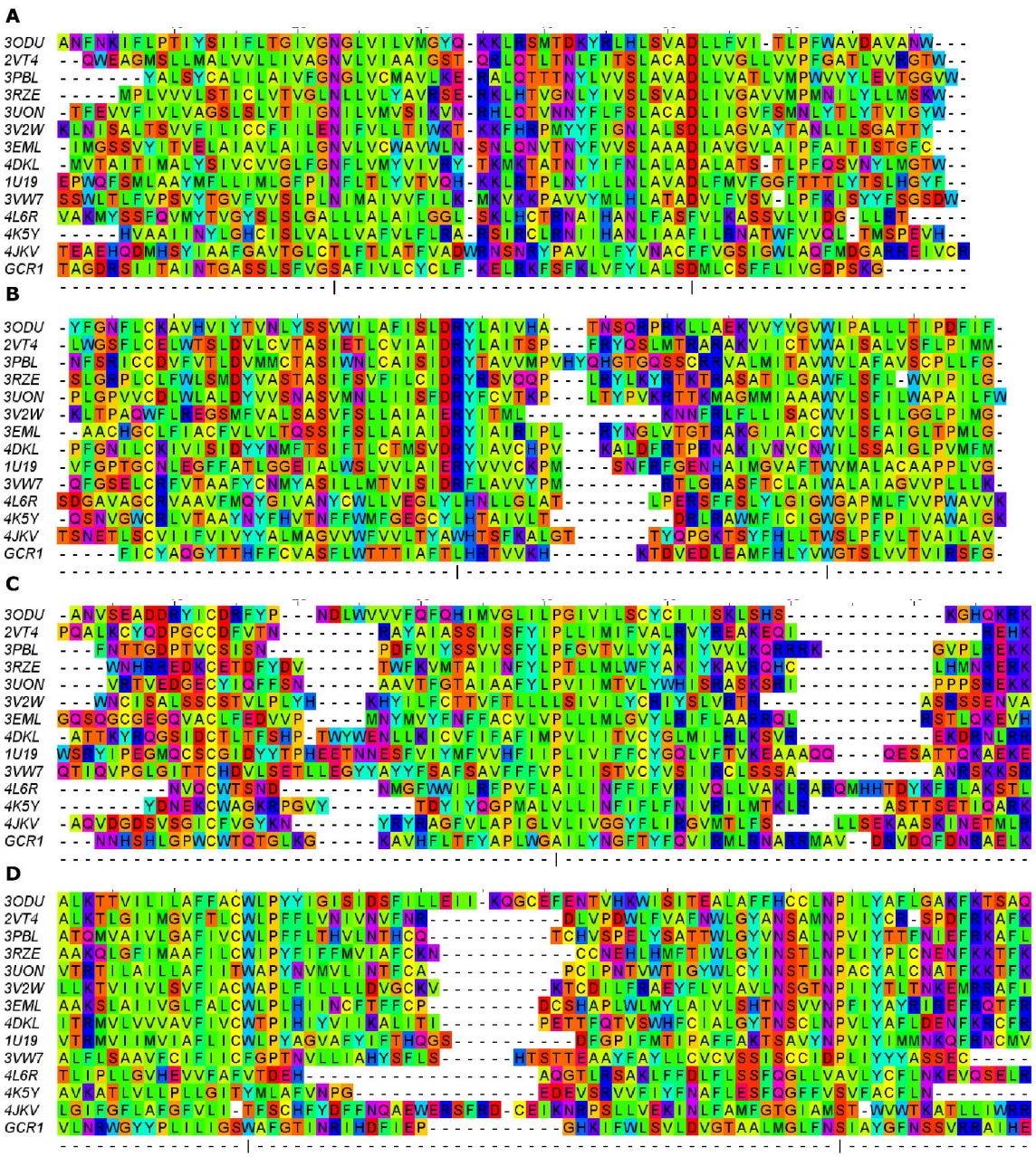
A
3ODU
2VT4
3PBL
3RZE
3UON
3V2W
3EML
4DKL
1U19
3VW7
4L6R
4K5Y
4JKV
GCR1
B
3ODU
2VT4
3PBL
3RZE
3UON
3V2W
3EML
4DKL
1U19
3VW7
4L6R
4K5Y
4JKV
GCR1
C
3ODU
2VT4
3PBL
3RZE
3UON
3V2W
3EML
4DKL
1U19
3VW7
4L6R
4K5Y
4JKV
GCR1
D
3ODU
2VT4
3PBL
3RZE
3UON
3V2W
3EML
4DKL
1U19
3VW7
4L6R
4K5Y
4JKV
GCR1

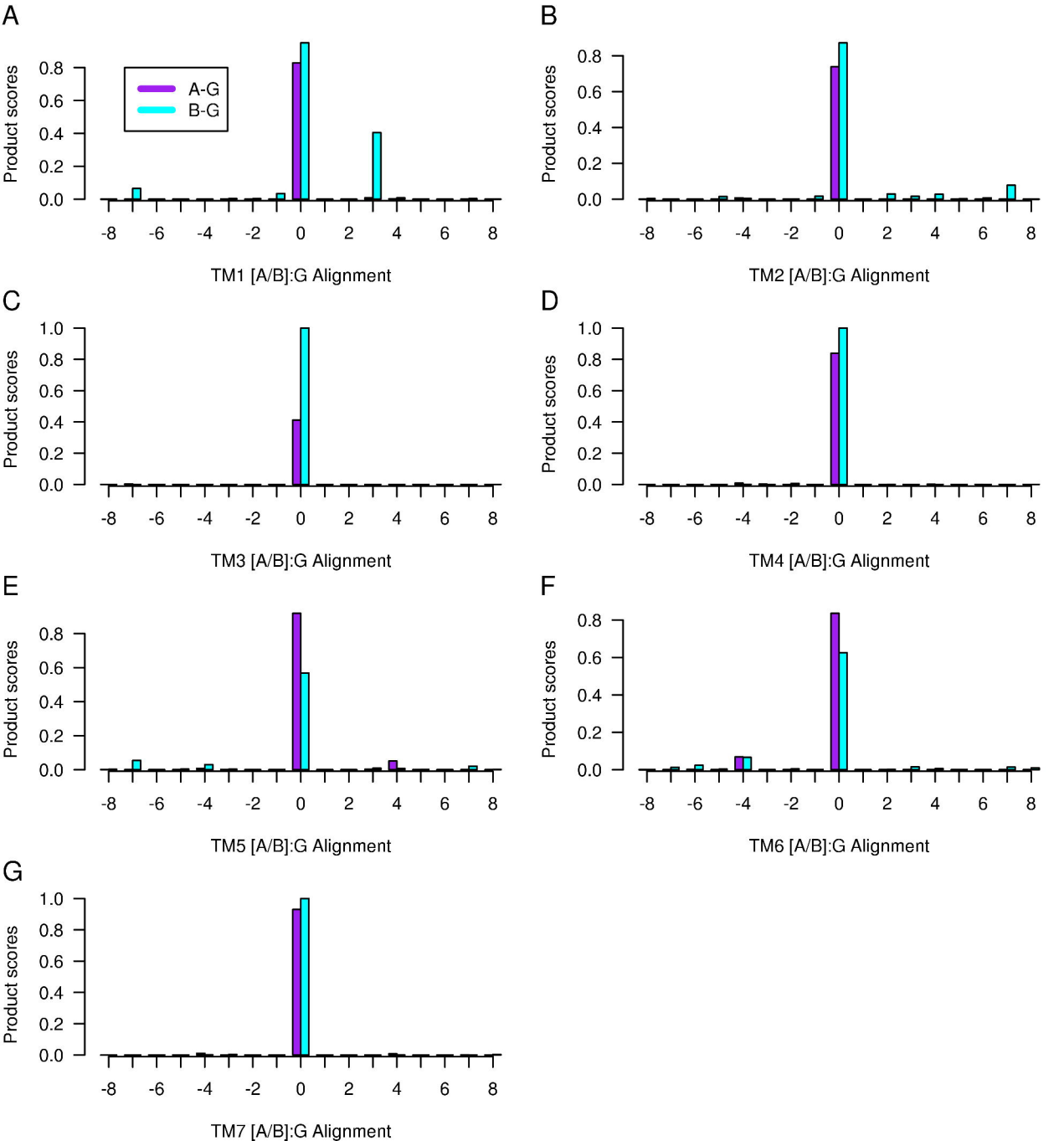
A
B
C
D
E
F
G
Product scores
A-G
B-G
TM1 [A/B]:G Alignment
TM2 [A/B]:G Alignment
TM3 [A/B]:G Alignment
TM4 [A/B]:G Alignment
TM5 [A/B]:G Alignment
TM6 [A/B]:G Alignment
TM7 [A/B]:G Alignment

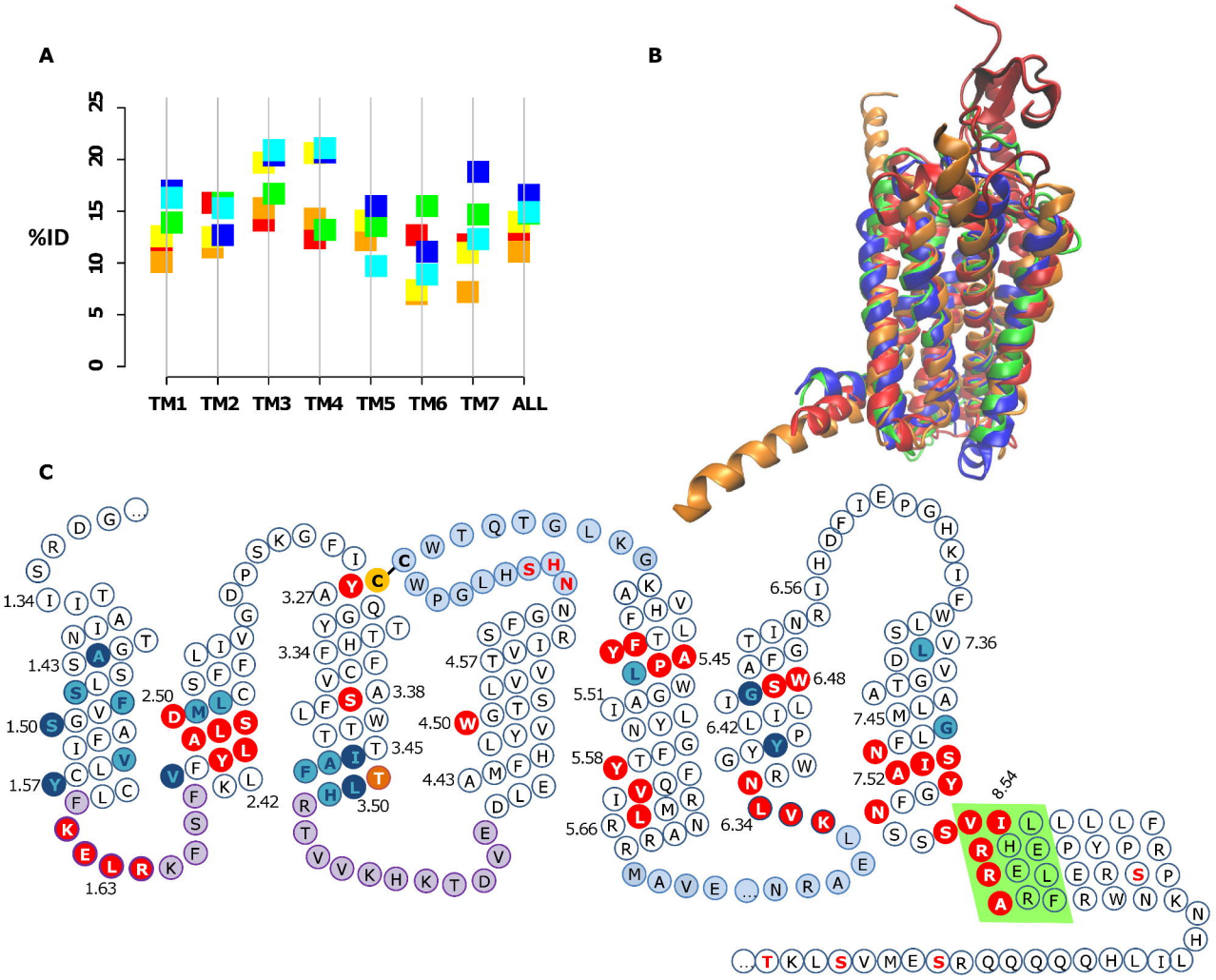
A
%ID
0
5
10
15
20
25
TM1
TM2
TM3
TM4
TM5
TM6
TM7
ALL
B
C
1.34
1.43
1.50
1.57
1.63
2.50
2.42
3.27
3.34
3.38
3.45
3.50
4.57
4.50
4.43
5.51
5.58
5.66
5.45
6.56
6.48
6.42
6.34
7.36
7.45
7.52
8.54

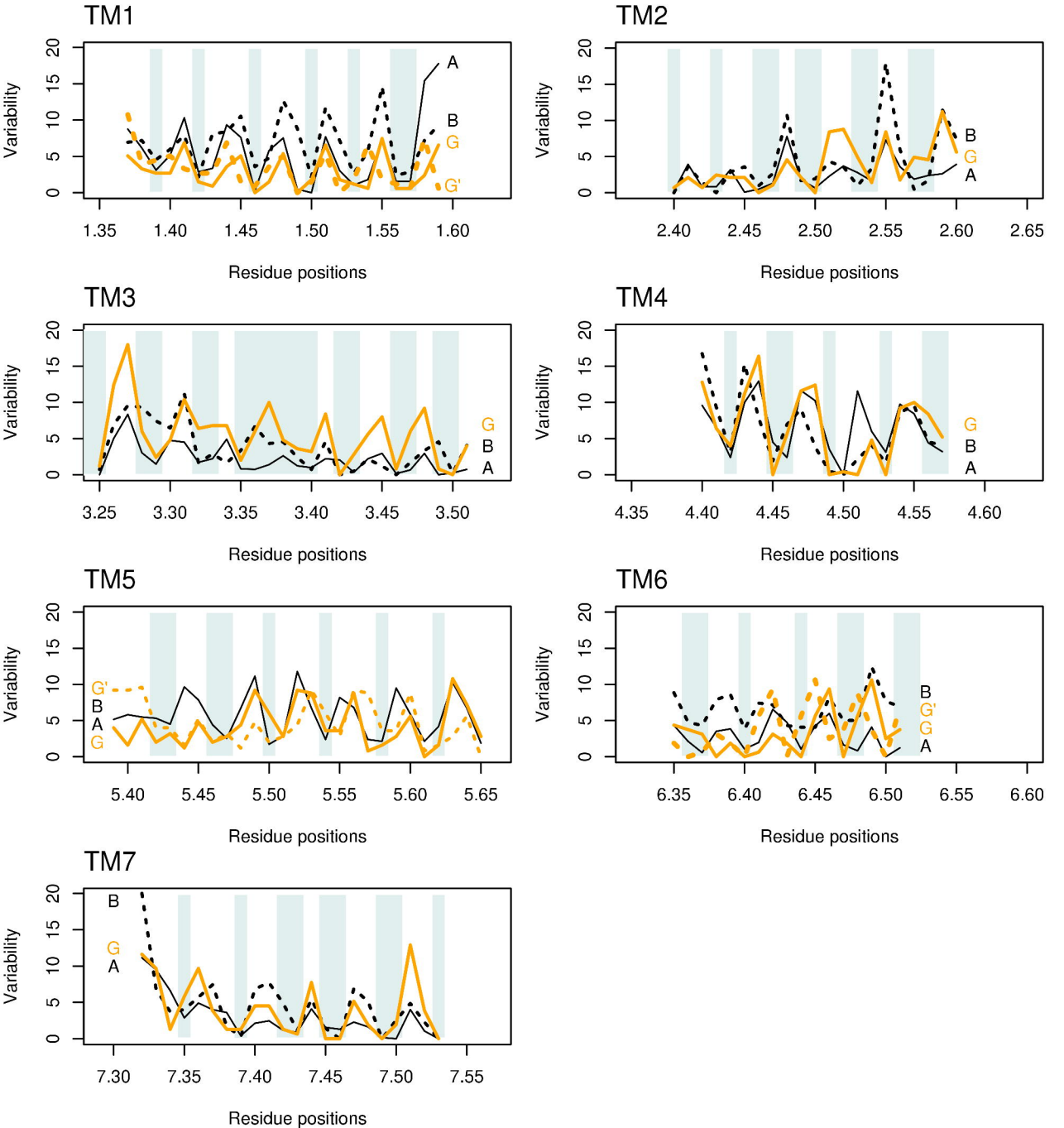
TM1
Variability
0
5
10
15
20
A
B
G
G'
1.35
1.40
1.45
1.50
1.55
1.60
Residue positions
TM2
Variability
0
5
10
15
20
B
G
A
2.40
2.45
2.50
2.55
2.60
2.65
Residue positions
TM3
Variability
0
5
10
15
20
G
B
A
3.25
3.30
3.35
3.40
3.45
3.50
Residue positions
TM4
Variability
0
5
10
15
20
G
B
A
4.35
4.40
4.45
4.50
4.55
4.60
Residue positions
TM5
Variability
0
5
10
15
20
G'
B
A
G
5.40
5.45
5.50
5.55
5.60
5.65
Residue positions
TM6
Variability
0
5
10
15
20
B
G'
G
A
6.35
6.40
6.45
6.50
6.55
6.60
Residue positions
TM7
Variability
0
5
10
15
20
B
G
A
7.30
7.35
7.40
7.45
7.50
7.55
Residue positions

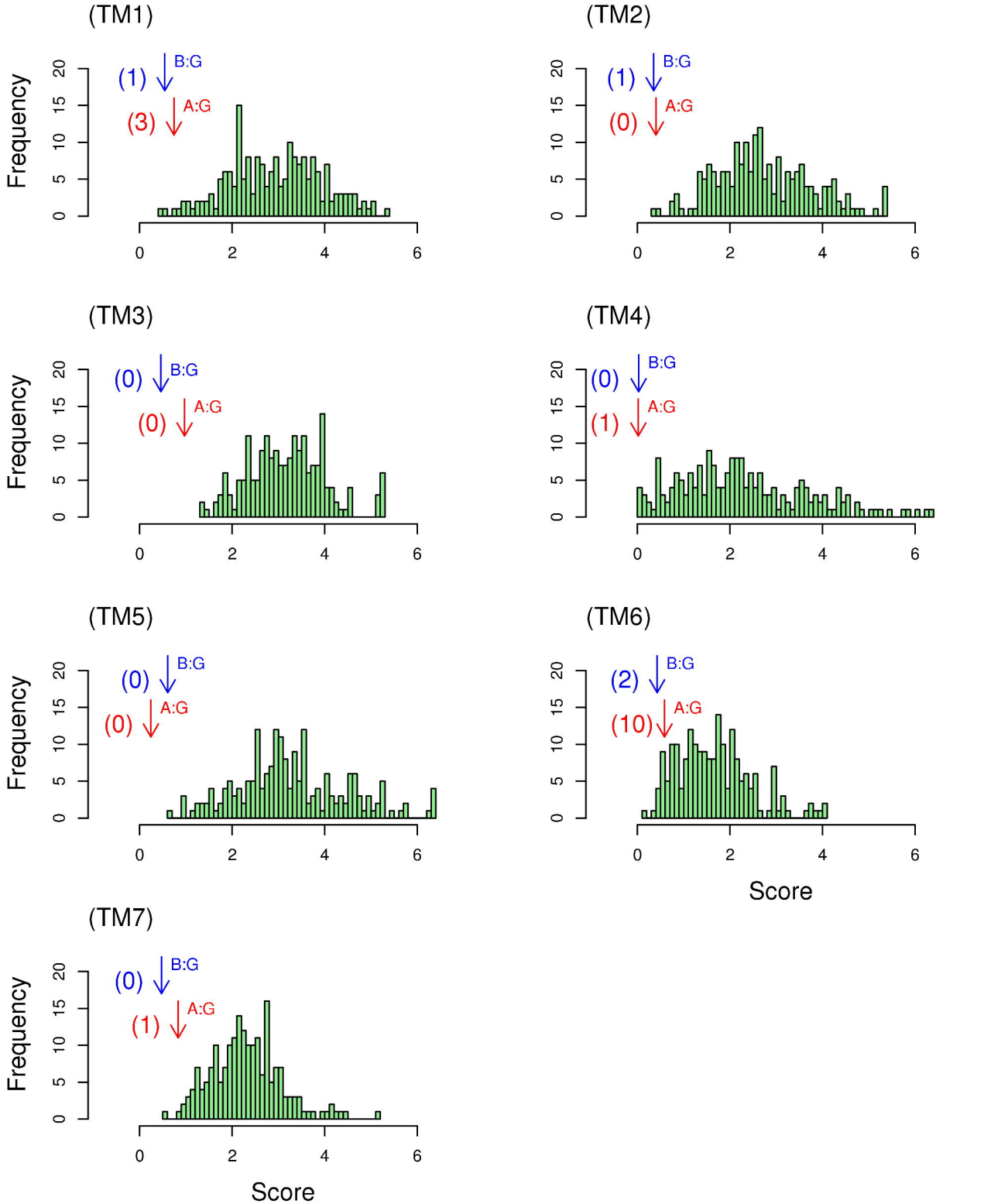
(TM1)
(1) B:G
(3) A:G
(TM2)
(1) B:G
(0) A:G
(TM3)
(0) B:G
(0) A:G
(TM4)
(0) B:G
(1) A:G
(TM5)
(0) B:G
(0) A:G
(TM6)
(2) B:G
(10) A:G
(TM7)
(0) B:G
(1) A:G
Frequency
Score
0
5
10
15
20
0
2
4
6